THESIS FOR THE DEGREE OF DOCTOR OF PHILOSOPHY IN
SOLID AND STRUCTURAL MECHANICS

Slab track optimisation considering dynamic train–track interaction

EMIL AGGESTAM

Department of Mechanics and Maritime Sciences

Division of Dynamics

CHALMERS UNIVERSITY OF TECHNOLOGY

Gothenburg, Sweden 2021

Slab track optimisation considering dynamic train–track interaction
EMIL AGGESTAM
ISBN 978-91-7905-454-0

Doktorsavhandlingar vid Chalmers tekniska högskola
Ny serie nr. 4921
ISSN 0346-718X
Department of Mechanics and Maritime Sciences
Division of Dynamics
Chalmers University of Technology
SE-412 96 Gothenburg
Sweden
Telephone: +46 (0)31-772 1000

Cover:
Slab track in the full-scale test rig at the Southwest Jiaotong University in Chengdu, China. The test rig was used in the calibration and validation process described in **Paper D**. Photo by Mr Jannik Theyssen.

Chalmers Reproservice
Gothenburg, Sweden 2021

Slab track optimisation considering dynamic train–track interaction

EMIL AGGESTAM
Department of Mechanics and Maritime Sciences
Division of Dynamics
Chalmers University of Technology

Abstract

Slab track is a type of railway track that is frequently used e.g. in high-speed applications as an alternative to ballasted track. Slab track is also well suited on bridges and in tunnels since no ballast is required and the cross-section of tunnels can be reduced. Slab tracks generally have lower maintenance demands than ballasted track. However, if maintenance is required it may be expensive and intrusive. On the other hand, overdimensioning of slab track will lead to high environmental impact and monetary cost. This thesis aims to increase the knowledge and improve the understanding of the dynamic interaction between vehicle and track in order to allow for the optimisation of slab track.

To this end, both two-dimensional (2D) and three-dimensional (3D) slab track models, and a transition zone model between slab track and ballasted track, have been developed. These models are used to simulate the vertical dynamic vehicle–track interaction in the time-domain. The computational cost of the simulation is reduced by using a complex-valued modal superposition technique for the finite element model of the track. In the 3D model, both rails are represented by beam elements, while the concrete parts are described using shell or solid elements. The simulations employ a mix of in-house and commercial codes. The influence of different irregularities, e.g. variations in track support conditions and irregularities in longitudinal level, on significant track responses such as wheel–rail contact forces, stresses in the concrete parts and pressure on the foundation is assessed. From Single-Input-Multiple-Output (SIMO) measurements carried out in a full-scale test rig, the 3D model has been calibrated and validated.

The developed models have been used to improve the designs of slab track and transition zones. Based on a multi-objective optimisation problem that is solved using a genetic algorithm, the transition zone design has been optimised to minimise the dynamic loads generated due to the stiffness gradient between the two track forms. The slab track design has been optimised to minimise the environmental footprint considering the constraint that the design must pass the static design criteria described in EN 16432-2. This design is then employed in the dynamic model where it is shown that there is a further potential for design improvements and related CO_2 savings. In particular, there may be possibilities to reduce the thickness of the concrete layers and the amount of concrete between the rails. Finally, a model of reinforced concrete has been implemented and combined with the dynamic model to assess consequences of cracking in the concrete panel and to evaluate stresses in the reinforcement bars.

Keywords: Slab track, dynamic vehicle–track interaction, transition zones, optimisation, genetic algorithm, modelling, measurement, ballastless track.

Preface

The work in this thesis has been accomplished from July 2016 to May 2021 at the Department of Mechanics and Maritime Sciences at Chalmers University of Technology within the research project TS19 "Design Criteria for Slab Track Structures". It has been a part of the research activities within the Centre of Excellence Chalmers Railway Mechanics (CHARMEC). In particular, the support from Trafikverket (the Swedish Transport Administration) and Abetong AB is acknowledged. Parts of the funding was provided by the European Union's Horizon 2020 research and innovation programme in the projects In2Track2 and In2Track3 under grant agreements Nos 826255 and 101012456. Several simulations have been performed on resources at Chalmers Centre for Computational Science and Engineering (C3SE) provided by the Swedish National Infrastructure for Computing (SNIC).

Acknowledgements

First of all, I would like to thank my main supervisor Prof Jens Nielsen, who has supported me within the project from day one. To me, you are the best supervisor a PhD-student can have. Throughout the project, you have always supported me with everything from guidance on how to proceed with a difficult task to careful proofreading. I really feel that you care for me and my project! Secondly, I want to thank my co-supervisors Prof Anders Ekberg and Dr Rikard Bolmsvik. Thank you, Anders, for your expertise in fatigue and fracture mechanics, and thank you, Rikard, for providing me with realistic input data for my models and helping me understand how to make the project beneficial for the industry. Cracking of reinforced concrete is a complex process, and I would like to thank Prof Karin Lundgren and Assoc. Prof Kamyab Zandi for your support in this subject.

I want to thank Assoc. Prof Shengyang Zhu and Prof Wanming Zhai from the Southwest Jiaotong University in Chengdu, China, for welcoming me to your university. I am very grateful for our cooperation when we conducted measurements in your excellent testing facility. I would like to express my gratitude to Mr Jannik Theyssen for helping me with conducting the measurements in Chengdu and for our collaboration when we wrote our joint paper. I really enjoy working and travelling with you!

I would also like to thank all of the members of the reference group. In particular, I am grateful to Dr Martin Li and Dr Andreas Andersson from Trafikverket for all your excellent questions and our fruitful discussions, which have increased the quality of my work. Also, I want to thank all the friends and colleagues at the Division of Dynamics and the Division of Material and Computational Mechanics. The work would not have been the same without the great atmosphere.

Furthermore, I would like to thank my mother, father and sister for always being there for me. Finally, I would like to express my deepest gratitude to my wife, Ida, and our children Signe and Olle. Thank you for all the love and support you surround me with.

Trollhättan, May 2021
Emil Aggestam

Thesis

This thesis consists of an extended summary and the following appended papers:

Paper A E. Aggestam, J. C. O. Nielsen and R. Bolmsvik. Simulation of vertical dynamic vehicle–track interaction using a two-dimensional slab track model. *Vehicle System Dynamics.* **56**(11) (2018), 1633–1657.

Paper B E. Aggestam and J. C. O. Nielsen. Multi-objective optimisation of transition zones between slab track and ballasted track using a genetic algorithm. *Journal of Sound and Vibration.* **446** (2019), 91–112.

Paper C E. Aggestam and J. C. O. Nielsen. Simulation of vertical dynamic vehicle–track interaction using a three-dimensional slab track model. *Engineering Structures.* **222** (2020), 110972.

Paper D J. Theyssen, E. Aggestam, S. Zhu, J. C. O. Nielsen, A. Pieringer, W. Kropp and W. Zhai. Calibration and validation of the dynamic response of two slab track models using data from a full-scale test rig. *Engineering Structures.* **234** (2021), 111980.

Paper E E. Aggestam, J. C. O. Nielsen, K. Lundgren, K. Zandi and A. Ekberg. Optimisation of slab track design considering dynamic train–track interaction and environmental impact. *To be submitted for international publication.* (2021).

The appended papers were prepared in collaboration with the co-authors. In **Paper A** – **Paper C** and **Paper E**, the author of this thesis was responsible for the major progress of the work including taking part in the planning of the papers, developing the theories and the numerical implementation, performing the numerical simulations and writing the papers. In **Paper D**, the planning and realisation of the measurements, the numerical simulations and the writing of the paper were conducted in close collaboration with Mr Jannik Theyssen.

Other publications by the author

- E. Aggestam, J. C. O. Nielsen and N. Sved. Simulation of vertical dynamic vehicle–track interaction – Comparison of two- and three-dimensional models. *Proceedings of the 26th International Symposium on Dynamics of Vehicles on Roads and Tracks, (IAVSD 2019), Gothenburg, Sweden, August 12–16, 2019*. Ed. by M. Klomp et al. Springer International Publisher. (2020), 415–422.

- E. Aggestam, J. C. O. Nielsen, A. Andersson and M. Li. Multi-objective design optimisation of transition zones between different railway track forms. *Proceedings of the 11th International Conference on Contact Mechanics and Wear of Rail/Wheel Systems (CM 2018), Delft, The Netherlands, September 24–27, 2018*. Ed. by Z. Li and A. Nunez. Delft University of Technology. (2018), 1–6.

- E. Aggestam. Simulation of vertical dynamic interaction between railway vehicle and slab track. Licentiate thesis. Department of Mechanics and Maritime Sciences. Chalmers University of Technology, Gothenburg, Sweden. (2018).

- E. Aggestam and J. C. O. Nielsen. Dynamic interaction between vehicle and slab track – Influence of track design parameters. *Proceedings of the 25th International Symposium on Dynamics of Vehicles on Roads and Tracks, (IAVSD 2017), Rockhampton, Australia, August 14–18, 2017*. Ed. by M. Spiryagin et al. Taylor & Francis Group. (2018), 699–704.

- E. Aggestam, F. Larsson, K. Runesson and F. Ekre. Numerical model reduction with error control in computational homogenization of transient heat flow. *Computer Methods in Applied Mechanics and Engineering*. **326** (2017), 193–222.

Contents

Part I
Extended summary

1 Introduction

When comparing the environmental impact from different modes of transportation, railway transportation has great potential. However, to make railway transportation competitive, traffic at higher speeds and/or higher axle loads is essential. On the other hand, this will also increase the loading of trains and track and increase costs for maintenance. New innovative track structures can be used, where the so-called slab track (also often referred to as non-ballasted track or ballastless track) is one of the most promising designs. In this chapter, high-speed railway lines, and slab track in particular, are first introduced in Sec. 1.1. The aim and limitations of the research are presented in Secs. 1.2 and 1.3.

1.1 Background

The use of railway transportation has increased significantly in recent decades [1]. In particular, the construction of new high-speed lines has grown worldwide, see Fig. 1.1. Travel time is one of the most important parameters for high-speed railway systems to be a competitive transport mode. To reduce travel time, the railway industry strives towards higher train speeds. During the last 50 years, the operational speed has increased significantly, and today, speeds up to 350 km/h are common [2].

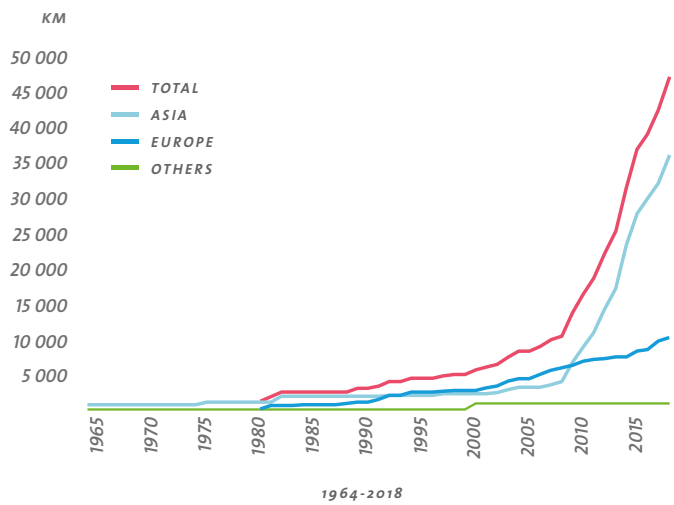

Figure 1.1: Total length of the high-speed railway network worldwide. From UIC [1].

Traditionally, ballasted track has been the dominating track form in the railway network. In a ballasted track, the rails are mounted on sleepers (beams usually made of wood or concrete) supported by ballast. A disadvantage of this type of track is that the track geometry may have a high degradation rate leading to the need for frequent maintenance [3, 4]. To mitigate the deterioration of the track, alternative track designs have been developed.

In Fig. 1.2, the designs of a slab track and a ballasted track, both developed for high-speed applications, are compared. In slab tracks, the sleepers are replaced or combined with large rectangular concrete plates. By installing these plates, a more robust structure is obtained which has a longer service life and requires less maintenance work. This leads to higher accessibility, which is an important factor since the interest in travelling by train is increasing. In addition, the lateral resistance of the track is increased and problems associated with degradation of ballast are eliminated [4]. However, a major disadvantage of slab track compared to ballasted track is that the environmental footprint of the construction is larger due to the significant required amounts of steel and concrete. Other disadvantages of slab track include higher construction cost, lower vibration/noise absorption and more expensive and intrusive maintenance in case it should be required.

(a) (b)

Figure 1.2: High-speed railway lines built using (a) slab track design (from STA [5]) and (b) ballasted track design (from UIC [1]).

1.2 Aim of research

In order to increase train speeds, and thus making railway transportation even more competitive, the slab track design has to be optimised. In particular, the optimised design needs to strike the delicate balance between having a high-quality track and the environmental and monetary costs of having an overdesigned solution. The impact of increased dynamic loads due to higher speeds can be assessed using simulations of dynamic vehicle–track interaction. In this thesis, the aim is to improve the understanding of the

vertical dynamic vehicle–track interaction when slab tracks are used. To this end, the following steps have been completed:

- Development of methodologies to simulate the vertical dynamic vehicle–track interaction when using (i) a two-dimensional (2D) slab track model (**Paper A**), (ii) a transition zone model between slab track and ballasted track (**Paper B**) and (iii) a three-dimensional (3D) slab track model (**Paper C**).
- Calibration and validation of the 3D slab track model (**Paper D**).
- Optimisation of (i) the stiffness gradient in a transition zone between slab track and ballasted track (**Paper B**) and (ii) slab track design (**Paper E**).

In Fig. 1.3, a flowchart is presented. The figure illustrates how the different papers are connected.

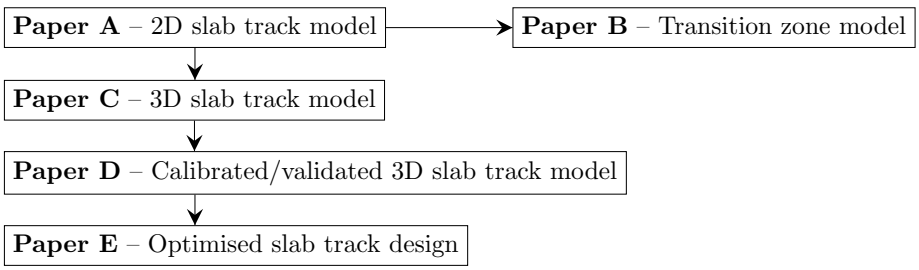

Figure 1.3: Flowchart of how the appended papers are connected.

1.3 Limitations

To limit the scope of the thesis, the research has been subjected to the following limitations:

1. Only linear elastic material models are considered.
2. Modelling of lateral and longitudinal dynamics are not included.
3. Slab track systems with rectangular-shaped panels are studied exclusively.
4. Development of differential settlement is not considered.
5. Full bond between concrete and steel is assumed.

2 Design of slab track structures

In this chapter, both high-speed railway lines in general and different slab track systems are described and discussed. In particular, Sec. 2.1 gives a brief review of the history of the development of railway lines, current designs of high-speed railway lines and what challenges the railway community needs to handle to make transport of freight and people by train a competitive option compared to other transport modes. In Sec. 2.2, an overview of different types of slab track systems is presented. The emphasis in this section lies in the description of slab track systems that use prefabricated concrete slabs since this is the type of system that is modelled and simulated in the appended papers. Finally, the requirements for slab track design presented in the European standard 16432-2 [6] are described in Sec. 2.3.

2.1 High-speed railway lines

The construction of railways started in the early 19th century during the industrial revolution [7]. One of the most famous projects was the so-called "Rocket" locomotive that travelled at 50 km/h and was designed by George Stephenson in 1829. Already in the beginning of the 20th century, top speeds over 200 km/h were recorded. However, in the 1930s, the average line speed between two cities was still only 135 km/h. In 1964, the first high-speed line, called Shinkansen, started to operate in Japan at train speed 210 km/h (later increased) over a distance of 515 km[1]. Initially, only ballasted track was used, but in 1972 the first sections of slab track were installed, and by 1993 over 1 000 km of slab track had been implemented in Japan [8]. In 1981, the first high-speed line in Europe started operating in France with a vehicle speed of 260 km/h, and it was built using ballasted track [7]. From the 1980s and onwards, several countries have built high-speed lines. In particular, China has since 2008 built a significant amount of high-speed lines (mainly built using slab track) and today Asia is carrying more than half of the high-speed railway traffic in the world [1]. The selection of track type is a complex task, see Ch. 3, where some countries, e.g. Germany, Japan and China, prefer to use slab track, while other countries, e.g. France, prefer ballasted track. The high-speed railway networks in Europe and Asia (including planned systems and systems under construction) are illustrated in Figs. 2.1 and 2.2, respectively.

High-speed railway lines are complex systems including infrastructure, stations, rolling stock, operations, maintenance strategies, financing, marketing and management. On top of that, railway lines may be different between different countries in terms of commercial approach, operational criteria and cost management [7]. However, high-speed railways is still a competitive mode of transportation since it offers high capacity and is environmentally sustainable. When high-speed lines are used, specialised trains and railway lines

[1]Today, the criterion for a high-speed railway line is operating speeds of at least 250 km/h [7]. Even though the Shinkansen originally operated at 210 km/h, it is commonly referred to as the first high-speed line.

are required. For these trains, the reliability, aerodynamics and dynamic characteristics are increased, whereas for the tracks, the track quality, catenary, and track layout are improved.

During recent decades, the design of ballasted tracks has improved significantly. In parallel, alternative track designs have been developed that need to be considered when new high-speed lines are built. In order for the railways to be further improved and stay as a competitive transport mode in the future, the UIC (International Union of Railways) states that one key aspect is that the slab track technology needs to be further assessed [7]. Today, it is a difficult task to determine whether slab track or ballasted track is the most beneficial track design for high-speed lines, see Ch. 3. In the decision process, several different parameters need to be taken into account, where the most important parameters are operational conditions (traffic characteristics), technical infrastructure features (viaducts, tunnels, local geotechnical features), environmental conditions (noise, vibration, CO_2 footprint) and cost.

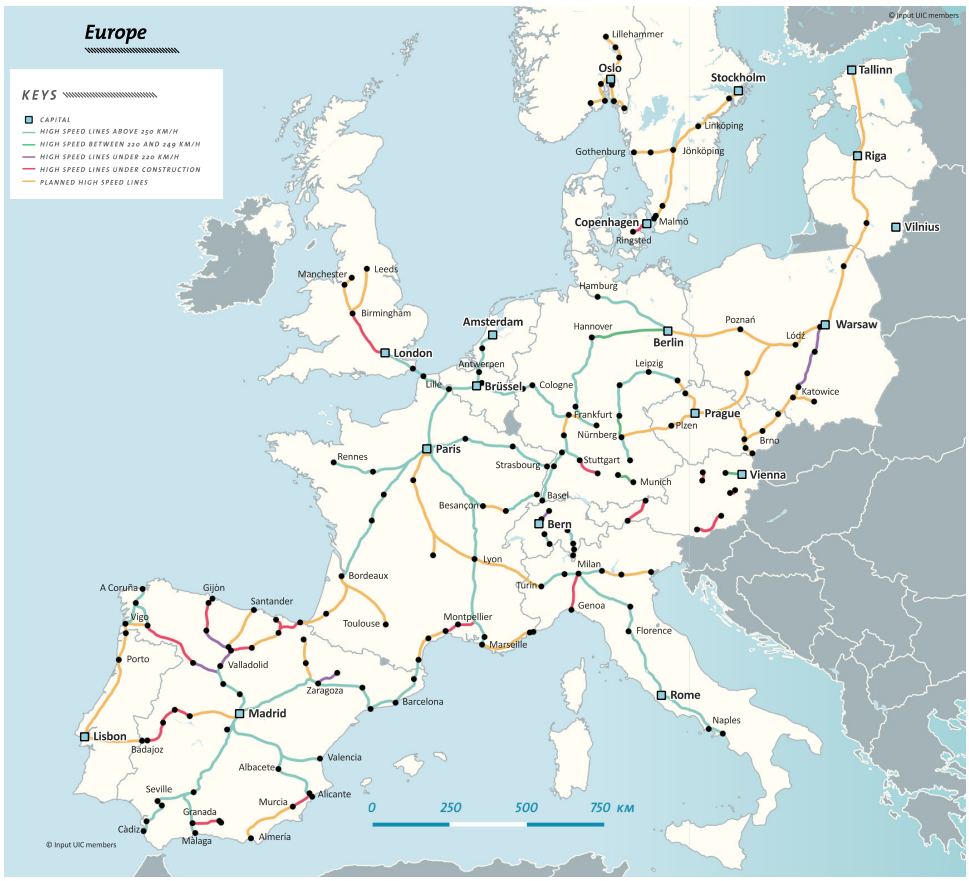

Figure 2.1: High-speed railway lines in Europe (2018). From UIC [1].

Figure 2.2: High-speed railway lines in Asia (2018). From UIC [1].

2.2 Survey of slab track systems

Although the use of slab track structures for high-speed applications has grown during recent decades, the technology is in several aspects similar to the original system that was installed in Japan 1972 [8]. However, during these years when the technology has been optimised, several types of slab track systems have been developed spanning from continuously supported systems with embedded rails to discretely supported systems with prefabricated concrete slabs. Extensive surveys including advantages and drawbacks of different slab track systems are presented in Refs. [2, 3, 9, 10].

In Fig. 2.3, the different types of slab track systems are summarised. In this thesis, the focus is on slab track systems where concrete slabs are used. An alternative to using concrete slabs is to use discrete sleepers or blocks on an asphalt layer [10]. Asphalt has several advantages compared to concrete, e.g. better noise absorption and possibility to adapt to stresses by plastic deformations [3]. The usage of slab tracks where the concrete slab is replaced with an asphalt layer is, however, small and therefore not studied in this thesis. Concrete slab systems can be further divided into discretely supported rail

systems, see Sec. 2.2.1, and continuously supported rail systems, see Sec. 2.2.2.

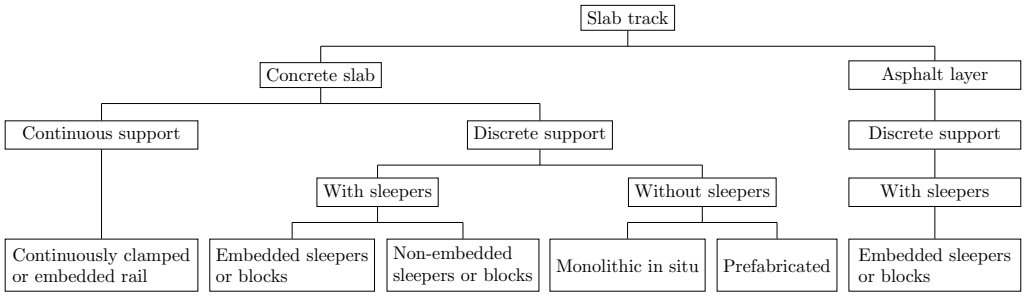

Figure 2.3: Different types of slab track designs. Inspired by Fig. 2 in Ref. [10].

2.2.1 Discretely supported rail systems

In discretely supported rail systems, which are the systems that dominate high-speed slab track lines, the rails are supported at discrete, equidistant locations. These systems can be further divided into systems with or without sleepers [3, 10].

When sleepers are used, they are either embedded in the slab or placed on top of the slab. One of the most well-known designs with sleepers embedded in the slab is the so-called Rheda system [3]. The first application was developed in the 1970s, and in 2000 an upgraded version of Rheda, called Rheda 2000, was installed. In Rheda 2000, the sleepers consist of a concrete filigree twin-block design, which ensures a precise location of the rails. The sleepers are embedded in a concrete slab, which is supported by a hydraulically bound layer (HBL). Today, Rheda 2000 has successfully been installed in Germany, the Netherlands, Taiwan and Korea [4]. Rheda 2000 and prefabricated slab track systems (that will be discussed below) are commonly called compact systems since the height of the superstructure is small compared to other systems.

When sleepers are not used, monolithic slabs or prefabricated concrete slabs are employed. Continuous monolithic slab track structures, which are particularly well suited for civil structures such as bridges, are not built on any larger scale for high-speed railway lines. In this thesis, the focus is instead on the modelling of prefabricated concrete slab track structures. This type of slab track is chosen since it is the most spread and common type of slab track in the world. When comparing prefabricated slab track systems to other slab track designs, the main advantages are that prefabricated systems are maintenance-friendly, have a high quality due to a high level of automation during production and a short construction time [3]. The main drawbacks of prefabricated slab track systems include difficulties in changing damaged slabs and small adaptability to large differential settlement in the embankment [11]. Today, several different prefabricated slab track structures are available on the market, where the most well-known designs are the Shinkansen, Feste Fahrbahn Bögl (FFB), ÖBB-Porr (also called Slab Track Austria, STA) and the China Railway Track System (CRTS) series. Two examples of the STA

system are shown in Figs. 2.4 and 2.5. Fig. 2.4 illustrates a system during construction, whereas Fig. 2.5 illustrates a system ready for traffic.

Below, a summary of the four most widespread prefabricated slab track systems is presented. The typical layers used in prefabricated slab track systems are shown in Fig. 2.6, and contain (from top to bottom); rails, fastening system, prefabricated concrete panels, (elastic slab mats), filling, concrete roadbed, (frost protection layer) and foundation/soil[2].

Figure 2.4: The STA system during construction. Note that the asphalt used as a base layer for the track in the photo is normally not used by STA. From STA [5].

Shinkansen

The development of the Shinkansen slab track started in the 1960s, and the first high-speed railway line using this type of slab track (which was the first commercially used high-speed slab track in the world) started operation in the 1970s [3]. Each prefabricated concrete panel of the Shinkansen slab track is approximately 5 m long and has a semi-circular cut (with a radius of 0.3 m) at the lateral centre of both ends in the longitudinal direction. When the prefabricated slabs are put together, circles are formed, where bollards are placed in order to prevent movements in the lateral and longitudinal directions.

[2]The layers within parentheses are not always installed depending on the geographical location and the design of the slab track.

Figure 2.5: Final STA system ready for traffic. From STA [5].

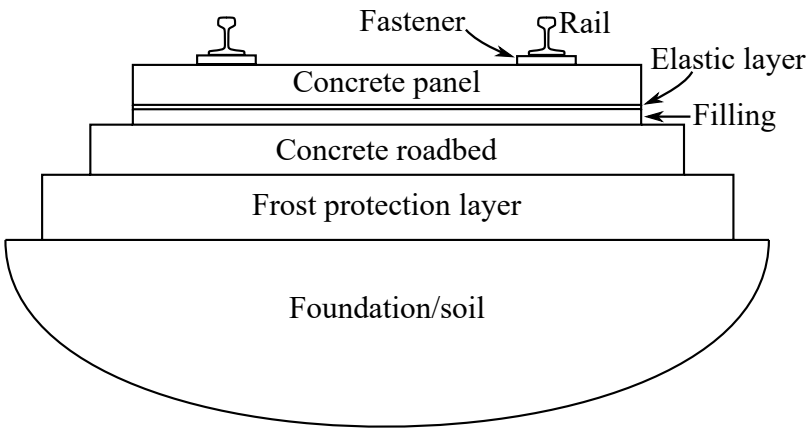

Figure 2.6: Schematic cross-section of a prefabricated slab track system.

Feste Fahrbahn Bögl

In the Feste Fahrbahn Bögl (FFB) slab track design, the reinforcement of the prefabricated panels with length 6.45 m is extended and coupled in the longitudinal direction to the reinforcement of the adjacent panels during construction [3]. By using such a design,

the final installation of the individual panels can be seen as one continuous panel that rests on the filling (bituminous-concrete mortar) and the roadbed (plain concrete). If the track is installed in a cold climate, a frost protection layer (FPL) is placed underneath the roadbed. In the FFB slab track design, no bollards are used which implies that longitudinal and lateral movements between the different layers are only prevented by friction. The slab track design by FFB has mostly been installed in Germany and China [4].

ÖBB-Porr

The slab track manufactured by ÖBB-Porr, sometimes also called Slab Track Austria (STA), has been a part of the railway infrastructure in Austria since 1989 and is today mostly used in Austria, Germany and Qatar [4]. STA uses a prefabricated concrete panel of length 5.2 m with two rectangular "holes". In these holes, self-compacting concrete (SCC) is poured during the construction (when the height of the panels has been fixed), which prevents movement in the longitudinal and lateral directions. An elastic layer is integrated at the bottom of the panel to allow for quick panel replacements and to reduce ground vibrations. Similar to the FFB system, the STA system rests on a concrete roadbed (which in the STA design is reinforced), and if the track is installed in a cold climate, an FPL is placed between the roadbed and the foundation.

China Railway Track System

The China Railway Track System (CRTS) series consists of three generations of slab track designs, which are usually denoted CRTS-I, CRTS-II and CRTS-III. In all these designs, the rail is discretely supported by a reinforced concrete panel [12]. The CRTS-I consists of discrete panels of 5 m and uses bollards to prevent motion in the lateral and longitudinal directions (similar to the Shinkansen design), whereas CRTS-II and CRTS-III are continuous with longitudinal joints (similar to the FFB design). In all the designs, the panels rest on a filling layer, a roadbed made of concrete (reinforced concrete for CRTS-I, and plain concrete for CRTS-II and CRTS-III) and a subgrade made of crushed stones. For CRTS-I and CRTS-II, the filling is made of cement-asphalt (CA) mortar, whereas self-compacting concrete is used for the CRTS-III. In **Paper D**, two slab track models have been calibrated versus dynamic measurements on a CRTS-III design.

2.2.2 Continuously supported rail systems

In continuously supported rail systems, the rail is continuously clamped or embedded in an elastomeric layer [3]. By using a continuously supported rail system, the dynamic loads are reduced compared to discretely supported rail systems due to the absence of the periodic variation in track stiffness from the discrete rail seats. Further, the degradation of the rails is reduced, and the need for maintenance is lower compared with other types of slab tracks. One disadvantage of continuously supported rail systems is that differential settlement of the foundation must be reduced to a minimum due to a minimal possibility of rail readjustment.

Continuously supported rail systems can be divided into embedded rail systems, also called embedded rail structures (ERSs), and rail structures that are clamped and continuously supported [3]. In ERSs, the rail is fixed by an elastic compound, typically cork or polyurethane, which surrounds the entire rail except for the rail head. During construction, the elastic compound is poured into the track using a groove. In the last 40 years, ERSs has been built in several pilot projects in the Netherlands. Although the benefits of the ERSs were verified in these projects, the usage of ERSs for high-speed lines is still rather limited (probably due to the requirement of settlement-free soil). In rail structures that are clamped and continuously supported, the rail is continuously supported without using any elastic compound. Examples of designs are the Cocon track and tracks using web-clamped rails [3]. The usage of these designs is, however, limited and they have not been installed in high-speed lines.

2.3 Design based on the European standard

In the European standard 16432-2 [6], requirements and recommendations for slab track design are given. These requirements and recommendations cover the design of the rail, fastening system, prefabricated panel, pavement, unbound layers and substructure. The standard also covers different slab track configurations including both continuously and discretely supported rail systems, designs with or without prefabricated panels and designs with either single or multiple layers of concrete. In this thesis, the focus is on discretely supported rail systems that use prefabricated panels and have multiple layers of concrete since this configuration is the most common design used for high-speed slab track applications.

In addition to the requirements and recommendations given in the main text in the standard, a detailed analytical design calculation method is presented for different types of slab track. The calculation method can be divided into three different parts that analyses (i) the rail (ii) the prefabricated panel and roadbed and (iii) the substructure. In this thesis, the focus is on the second part dealing with the concrete parts. The main idea of this step in the analytical design calculation method is to compare calculated stresses with strength limits. In **Paper E**, this calculation model is used to optimise the thicknesses, widths and the type of concrete used in the slab track design.

The calculation method that is used to determine if a design passes all criteria is summarised in Fig. 2.7. In the initial step, data on the vehicle load, concrete parts and temperature loads have to be defined. The vehicle load is then used in a beam model of the rail to calculate the rail seat loads using a static model where the dynamics of the vehicle–track interaction is taken into account by using a dynamic amplification factor of 1.5 (independently of design train speed). The obtained rail seat loads are then applied in an analysis of the concrete parts, where both a beam model and a slab model are used. From these models, flexural stresses are calculated (in the longitudinal direction for the beam model and in both the lateral and longitudinal directions for the slab model). In the longitudinal direction, a conservative approach is used by selecting the maximum

calculated flexural stress from the beam and slab models. The calculated flexural stresses are then compared with the corresponding flexural strength limits from a fatigue model. By taking the ratios of the flexural strength limits and the corresponding flexural stresses, different safety factors (SFs) are calculated. If all of the calculated safety factors are larger than or equal to one, the design is approved. If not, a design evaluation has to be made, and the process has to be restarted for the revised design.

In order to pass the standard, there is a trade-off between having a thinner panel or a thinner roadbed. In Fig. 2.8, this trade-off is illustrated for three different types of concrete where the upper-right area corresponds to thickness combinations of the concrete layers that will pass the standard, while the lower-left area represents combinations that will not pass. In addition, the calculated design that has been optimised to minimise the environmental impact from slab track is shown. In the figure, it is seen that the lines have discontinuous derivatives at certain locations. These discontinuous derivatives occur since the limiting safety factor for the design is changed at these locations.

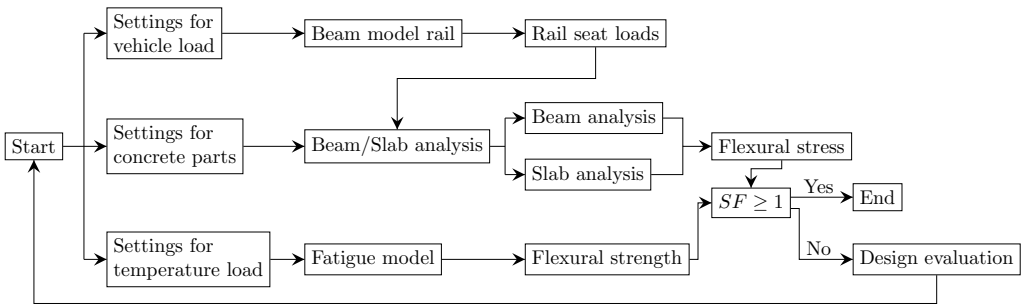

Figure 2.7: Steps in the analytical calculation model presented in the European standard 16432-2 [6] (from **Paper E**).

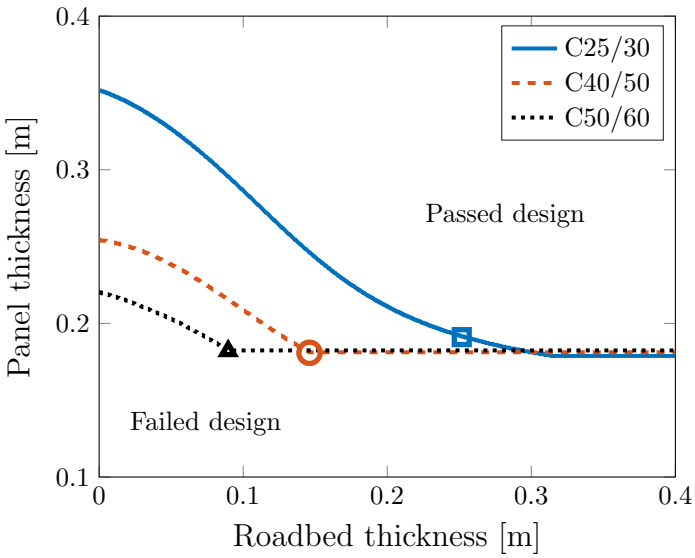

Figure 2.8: Combinations of panel and roadbed thicknesses that will pass or fail the European standard 16432-2 [6]. The markers in the figure highlight the optimised dimensions (from **Paper E**).

3 Slab track versus ballasted track

When comparing slab track and ballasted track, an advantage when using slab track is that the track geometry deteriorates at a slower rate and less maintenance work is required. Hence, the availability of a slab track can be expected to be higher, which increases the capacity if the track is fully utilised. However, when maintenance work on slab track is required, it is often more extensive compared to maintenance work on ballasted track. One of the main reasons why the deterioration rate is higher for the ballasted track is that the track structure is relatively soft in the lateral and longitudinal directions due to the discrete sleeper support. In particular, this is a problem in curves since the lateral resistance provided by the ballast is limited. Further, in the long-term, the high contact stresses occurring between sleeper and ballast may lead to displacement of the ballast, and thus uneven support of the sleepers [3]. The uneven support by the ballast, combined with dynamic loads from vehicles, cause movements of the sleepers which induce ballast degradation and differential track settlement. Poor quality of the track geometry leads to increased dynamic loads, which further increases the differential settlement. Another problem associated with the degradation of ballast is that fine particles are separated from the ballast stones due to wear and fracture, which may cause drainage problems.

If the vehicle speed is increased, the requirements on the track design become harder to meet. In particular, the minimum curve radius has to be increased. Therefore, more tunnels and bridges are typically required for high-speed lines. Slab tracks are particularly well-suited for tunnels and bridges since no ballast is required. On these rigid structures, the roadbed of the slab track is not required and, due to the low height of the superstructure, the cross-section of tunnels can be made smaller compared to ballasted track [13]. Further, the accessibility of road vehicles in tunnels, which is required in case of an emergency, is easier to integrate when using slab track compared to ballasted track [3].

In terms of the costs for slab track and ballasted track, the general conclusion is that slab track is more expensive to build, but requires less maintenance and has a longer service life. In a review paper by Matias and Ferreira [10], the initial cost of building different types of slab tracks has been compared with the cost of building ballasted track. There are large deviations in initial costs depending on which type of slab track that is considered. The ratio in cost compared to ballasted track ranges from 1.0 to 3.0. However, when considering prefabricated slab track systems, the initial cost ratio compared to ballasted track ranges from 1.3 to 2.0. Since the decision of whether building slab track or ballasted track may have tremendous economic effects, published results describing all the decisions made and including an assessment of the costs are limited [4, 14]. When comparing maintenance costs, Shiau et al. [15] state that the maintenance cost of slab track is approximately 10% of the maintenance cost of ballasted track. The maintenance cost will, however, vary significantly between different sites, and Ando and Sunaga [16] concluded that the maintenance cost of the Sanyo Shinkansen slab track line was 25% of the maintenance cost for a ballasted track. LCC (Life-Cycle Cost) analyses comparing ballasted track and slab track are, generally, not available since the input to

the analysis varies with topography, climate, operational conditions, discount rate, etc. [4, 17]. Further, when LCC analyses are performed, there are a lot of uncertainties, where the most critical ones that need to be assessed before a track is built, independently of track design, is the maintenance cost and the cost of building the track. Moreover, it shall be noted that ballasted track is a thoroughly tested track design that has been used for over 150 years [14]. Therefore, track engineers know what types of problems to expect and how to handle them.

Another important parameter that needs to be taken into account when comparing different track structures is the environmental footprint. A drawback when considering slab track is that more concrete is required. In addition, slab track requires more subsoil improvements to minimise differential settlements [13]. However, slab track may still be the best option for a railway line due to the longer service life and lower maintenance requirements [13, 18]. It should be noted that the rail steel, which is the same in both types of structures, causes roughly half of all of the carbon dioxide (CO_2) emissions. Finally, there is a potential to reduce the environmental footprint from slab track by using structural optimisation and considering the usage of alternative binders and materials [19].

In slab track design, the emphasis is typically put on the concrete panel, while the roadbed and foundation are designed using general platform design rules [4]. The requirements on the roadbed and foundation are, however, crucial since differential settlement of the slab track must not occur. In the European standard 16432-2 [6], limit values are provided for the modulus of deformation, E_{v2}, (which is a measure of the stiffness of the foundation) and the design of the roadbed thickness is included in the presented calculation method, see Sec. 2.3. For track on soft soils, the foundation stiffness can be increased by using a so-called settlement free plate (SFP), which is a viaduct-like structure that the slab track is placed on [4]. SFPs have successfully been used in the Netherlands and China.

Slab track is generally a stiffer structure than ballasted track. The track stiffness at the rail level of slab tracks is typically reduced by using a softer rail pad. Using a low-stiffness rail pad is, however, non-beneficial from an acoustic point of view since rail vibrations are increased due to reduced track decay rates [20]. Further, ballast is a good noise absorber, whereas the slab (if not treated) is a noise reflector. These noise problems lead to an overall noise increase of about 3 dB for slab tracks. Actions have been made to reduce the higher noise associated with slab tracks, e.g. by installing absorbing panels, but this is still an area that needs to be further investigated. For more information about the acoustic performance of slab tracks, see Ref. [21].

According to the United Nations, a well functional and sustainable infrastructure is crucial for humans in the future [22]. One step in order to achieve this is a state-of-the-art railway transport mode. However, due to the high installation cost of new track, the technologies used must be thoroughly investigated. To decide whether slab track or ballasted track should be used on a given line is a difficult question for the infrastructure manager. To increase the odds of making the right decision, all different aspects of building slab track and ballasted track have to be addressed.

4 Transition zones between different track forms

In a transition between two different track forms, there is a structural discontinuity that leads to an abrupt variation in the track stiffness and increased dynamic loads [23]. There is also a variation in track stiffness due to a transition between two different substructures, e.g. embankment to bridge or tunnel. Independently of the type of transition, the gradient in track stiffness generates increased dynamic loads that may lead to differential ballast/subgrade settlement and irregularities in track geometry (longitudinal level). The accumulated settlement and resulting degradation of track geometry magnify the dynamic loads further which creates a vicious circle. Hence, the track adjacent to a transition is prone to deteriorate at an accelerating rate, and frequent maintenance work is required. At transitions, the number of required maintenance actions may be three to eight times higher compared to a conventional uniform track [24]. Further, performing track maintenance work is a costly process. As an example from 2015, 54% of the investment cost (5199 million Euros) for infrastructure in Spain went to railways and a significant part of this sum was spent on maintenance of track and infrastructure materials.

To decrease the required maintenance work associated with transitions, various types of transition zones can be installed. In different countries, different approaches have been applied. For most of the approaches, the key idea is to reduce the dynamic loads by making the softer track stiffer and the stiffer track softer in the vicinity of the transition. In doing so, a smoother gradient in the vertical track stiffness can be achieved, and the degradation of the track is reduced. When considering transition zones between ballasted track and slab track, a smoothing of the vertical track stiffness can be achieved by improving the substructure, superstructure or a combination of these [2].

The substructure in a transition zone can be improved by enhancing the soil by implementation of geocells or geotextiles [24]. In addition, the stiffness of the soil can be increased significantly using piles. To mitigate low-frequency ground-borne vibrations, it can be beneficial to install under ballast mats. Finally, it is common to use a transition wedge solution, where there is a gradual change from softer to harder materials.

The superstructure can be improved in many different ways. To reduce vibrations and provide a smoother stiffness variation, it is common to use under sleeper pads (USP), under slab mats and to optimise the rail pad stiffness. The variation of stiffness can also be reduced by adding auxiliary rails, glueing of ballast, varying the sleeper length and width and/or the sleeper spacing close to the transition [2, 25]. The stiffness on the ballasted track can also be increased by using a so-called transition approach slab, which is a slab that is placed under the sleepers [24].

Regarding the length of the transition zone, a common requirement is that the length should be at least the distance that the vehicle travels during half a second [24]. However, based on results from **Paper B**, the length of the transition zone can be reduced significantly (at least in terms of reducing the dynamic loads induced by the stiffness

gradient).

To determine an optimal distribution of the vertical track stiffness at the transition is not trivial. The optimal vertical track stiffness depends on the operating conditions on the track, e.g. high-speed or freight [24]. A high stiffness increases the dynamic wheel–rail contact forces, whereas a low stiffness increases the energy dissipation, rail vibrations and noise. Further, the optimal distribution of the stiffness in a transition zone depends on what response is evaluated. As an example, to minimise settlement, a vertical track stiffness that gives a low dynamic load on the foundation is required. On the other hand, if a vehicle response, e.g. ride comfort, shall be optimised, another distribution of the vertical track stiffness may be optimal. Hence, there is a trade-off between achieving minima of different track and vehicle responses. How to optimise a transition zone when several track and/or vehicle responses are taken into account simultaneously is further elaborated in Ch. 8. Finally, for information about the modelling of transition zones, see Sec. 5.3.

5 Dynamic train–track interaction

When comparing the railway mode to other modes of transportation, one of the unique features is the interaction between wheel and rail, which is the main source of vibrations when a train runs over a track. Since the birth of railways, researchers have been trying to model these vibrations accurately in order to understand how to reduce the noise and the deterioration of the vehicle and the track. A historical survey of the modelling of vehicle–track interaction is described briefly in Sec. 5.1.

The modelling of the track can be performed using analytical or numerical models and can be evaluated in either the time domain or the frequency domain [26]. The major benefit of analytical models is that they are computationally cheaper, but they are not well suited to account for irregularities in vehicle, track and/or soil properties. Historically, analytical models have been used due to limited computational power, but nowadays numerical methods are commonly used. In Secs. 5.2 and 5.3, a review of different techniques for the modelling of the dynamic vehicle–track interaction is given for slab track systems and transition zones, respectively.

Whether a model in the time domain or the frequency domain is the most suitable option depends on the purpose of the simulation. Generally, analyses performed in the frequency domain are computationally cheaper than analyses in the time domain. However, to apply a frequency-domain model, the coupled vehicle–track system has to be taken as linear. In contrast, a problem with time-domain models is that frequency-dependent material parameters cannot be accounted for. In particular, the stiffness and damping of rail pads and under sleeper pads (USP) are known to be frequency-dependent.

When the vertical dynamic vehicle–track interaction is studied, irregularities in longitudinal level has a significant effect [27]. A particularly severe type of track irregularity is rail corrugation, which has been studied in detail e.g. by Correa et al. [28]. According to the European standard 13848-6 [29], the quality of a track can be assessed based on the standard deviation of irregularities in longitudinal level (in a specific wavelength interval). In the standard, five track quality classes are defined, spanning from A to E, for which speed-dependent limit values are provided. In **Paper E**, these limit values were used to investigate the impact of irregularities in longitudinal level on the dynamic loads.

In simulations of vertical dynamic vehicle–track interaction, irregularities in longitudinal level are usually represented by (a) measured irregularity profiles from the field or (b) using a Power Spectral Density (PSD) function. The PSD is a statistical function used to represent random track irregularities, and by using an inverse Fourier transform, samples of irregularities in longitudinal level as a function of longitudinal track position can be generated. The use of PSDs to quantify track irregularities is employed worldwide, and in the Handbook of Railway Vehicle Dynamics [30], comparisons of different PSDs used in different parts of the world are presented and compared. In this thesis, the influence of irregularities in longitudinal level on significant track responses has been studied using both measured irregularity profiles (**Paper C**) and PSDs (**Paper B** and **Paper E**).

In this thesis, a range of different finite element (FE) models of slab tracks has been developed. Within the models, different types of elements have been considered including beam, shell and/or solid elements. The track models can be classified into beam element models and shell/solid element models depending on how the concrete parts are modelled. In the beam element models used in this thesis, all parts which are described using finite elements are modelled using Rayleigh–Timoshenko beam elements, while a mix of different types of elements is employed in the shell/solid element models. Note that the rails are described using beam elements also in the shell/solid element models. When only beam elements are used to describe the track, the computational cost is relatively low. This approach is used in **Paper A** and **Paper B** and is summarised in Sec. 5.4. For all beam element models developed in this thesis, a symmetric track structure and a symmetric track excitation with respect to the centre of the track between the two rails are assumed. Hence, only one rail and half of the width of the slab need to be modelled, which implies that the model will be two-dimensional (2D). Note that even though the transition zone model in **Paper B** only consists of beam elements, it is still three-dimensional (3D) since the sleepers are placed perpendicular to the rail.

For the shell/solid element models, also referred to as the 3D models, both of the rails are modelled using beam elements, while the concrete parts are modelled using shell or solid elements, see **Paper C** – **Paper E** and Sec. 5.5. When using the 3D models, the influence of non-symmetric track excitations can be assessed, but the computational cost is increased.

How to model each part of the coupled vehicle–track system depends on what response is of main interest. For example, if a low-frequency vehicle response shall be analysed, the track model can generally be represented by a simple model of the track stiffness and damping in the frequency range of the vehicle response (typically up to 20 Hz). In the appended papers of this thesis, the focus is on the response of the track superstructure. Therefore, the vehicle model is simplified to a multibody system, see Sec. 5.6. In addition, it is assumed that the soil can be modelled as a Winkler-type foundation (non-interacting springs and viscous dampers). To study ground-borne vibrations, a more advanced model of the soil is required, cf. [31, 32].

To simulate the interaction between a vehicle and a track, the track and vehicle models should be coupled into one integrated system. Sec. 5.7 presents a summary of how the vertical dynamic vehicle–track interaction is simulated in this thesis.

5.1 Historical review

In this section, a brief review of the development of the modelling of dynamic vehicle–track interaction is given. More comprehensive reviews have been written by Knothe and Grassie [33] and Connolly et al. [26].

The first dynamic analysis of a track was carried out by Timoshenko in 1926 [34]. In this model, which handled the excitation by a harmonically varying stationary load, the

track was modelled as a continuously supported Euler–Bernoulli beam. This model was further advanced by describing the rail as a Timoshenko beam, cf. [35], and by modelling the sleepers as rigid bodies at discrete locations, cf. [36]. Timoshenko beam theory provides a more realistic response at high frequencies since shear deformation of the rail cross-section is taken into account. At the beginning of the 1990s, the use of finite element models and analyses performed in the time domain started to increase. These methods were, however, computationally demanding (in particular with the computational power that was available at that time). By using a modal analysis for the track model, the computational cost can be reduced. This was utilised by Lin and Tretheway [37] when solving the problem of a mass–spring–damper system moving on an elastic beam. By accounting for non-linear characteristics of the track and vehicle in time-domain analyses, the influence of various imperfections have been analysed using coupled models of vehicle–track dynamics, cf. [38–40]. Today, FE models analysing the dynamic vehicle–track interaction in the time domain are frequently used for a large variety of applications. In Secs. 5.2 and 5.3, these kinds of models are reviewed for slab track systems and transition zones, respectively.

5.2 Review of slab track models

For the modelling of dynamic vehicle–track interaction, Connolly et al. [26] describe that there are four cornerstones that are linked together: accuracy, usability, parameter availability and computational cost. Depending on the purpose of the simulation, and what cornerstones are considered most important, various simulation models can be used. Today, a common approach is to model the track using finite elements and the vehicle as a multi-body system. Zhai et al. [41] developed a 3D model to investigate the coupled vehicle–track system, both for ballasted track and slab track. The concrete slabs were modelled as elastic rectangular plates, and asymmetrical vertical irregularities for the two rails were considered. Galvín et al. [42] modelled the vehicle as a multi-body system, the track with finite elements and the soil using a boundary element method. Based on the coupled 3D model, displacements and velocities were calculated for the car body, the track components and for the soil in the free field. In several studies, the dynamic behaviour of a 3D slab track model has been validated against measurement data, see **Paper D** and Refs. [41–46].

Slab tracks have been modelled to analyse a variety of dynamic responses. For a floating slab track system, Li and Wu [47] investigated how the load transmission to the soil depends on the length of the slabs. Poveda et al. [48] analysed the fatigue life of slab track, and used the results to optimise the geometry of the slabs. Lei and Wang [49] modelled the track with finite elements and used a moving reference frame (the track model was assumed to be invariant along the track structure). In doing so, the vehicle acts at the same position on the rail throughout the simulation, and the study of the dynamic interaction between vehicle and continuous slab track can be solved at a lower computational cost. Zhu et al. [50] used a non-linear and fractional derivative viscoelastic (FDV) model of the rail pads to capture their complex characteristics. Coupled vehicle–

track interaction simulations were performed and compared to simulations where the rail pad was described by a traditional Kelvin model. For discontinuous slabs, Zhang et al. [51] calculated a range of different track and vehicle responses when taking track irregularities into account. In their work, the track and vehicle were coupled through a linearised wheel–rail contact force, and all simulations were performed in the frequency domain. Sadeghi et al. [44, 52] extended the model to three dimensions and included non-linear properties of the wheel–rail contact. Yang et al. [53] used a so-called composite track model (the track model was divided into repetitive track elements that were combined to assemble the entire track model) and analysed how various track responses were influenced by rail irregularities. In a work conducted by Zhu et al. [54], the vehicle model was included in the FE model, and a track designed to reduce low-frequency vibrations was developed.

In several papers, similarities and differences between slab track and ballasted track have been analysed. As examples, Blanco-Lorenzo et al. [55] analysed and compared ballasted track with various traditional slab track designs (Rheda 2000, STEDEF and a floating-slab track), whereas Bezin et al. [14] compared ballasted track with two innovative slab track designs (one steel-concrete slab track and one embedded slab track).

5.3 Review of transition zone models

Similar to the modelling of slab track systems, the modelling of transition zones can be achieved in various ways depending on the purpose of the simulation and the type of transition. As examples, simulations and measurements have been used to study transition zones between embankment and bridge, [23, 56], embankment over a culvert, [57, 58], and between slab track and ballasted track, [25, 42, 59].

The interest in the modelling of transition zones has grown in the last decade. One of the first analysis of transition zones was performed by Lei and Mao [60]. The influences of settlement and variations in the foundation stiffness and vehicle speed on the dynamic wheel–rail contact forces were investigated. It was concluded that the vertical irregularity due to settlement (modelled by changing the level of the rail) is the main source of the increased wheel–rail contact forces. However, the study only considered a ballasted track model and the transition zone was solely modelled by changing the rail level and/or foundation stiffness. For a transition zone between a ballasted track and a floating-slab track, Li and Wu [61] calculated rail displacements and wheel–rail contact forces and studied the influence of vehicle speed and the fundamental natural frequency of the floating-slab track. By combining the slab track and ballasted track models developed by Zhai et al. [41], a methodology was presented to simulate transition zones between ballasted track on an embankment and slab track on a bridge [43, 62]. Galvín et al. [42] used a coupled 3D FE model and boundary element model to simulate a transition zone between a ballasted track and a slab track. The transition zone was divided into four sections of varying track structure to smoothen the change in the vertical track stiffness, and the influence of the stiffnesses of the rail pads and foundation was investigated.

Shahraki et al. [25] used a simulation model to calculate rail displacements, velocities and accelerations to examine the dynamic performance of a transition zone from a ballasted track to a slab track when using longer sleepers, auxiliary rails and/or improved subgrade. The potential of using rubber mats in transition zones between two different slab track designs was investigated by Xin et al. [63]. Based on simulations of dynamic vehicle–track interaction, an optimised transition zone design was established. Zakeri and Ghorbani [64] investigated how the displacements and accelerations of the rail can be reduced by gradually reducing the thickness of the slab in the transition zone. Finally, Wang and Markine [65] used a 3D dynamic FE model, which was validated against field measurements, to study a bridge–embankment transition zone (in both travel directions). By combining the FE model with an empirical settlement model in an iterative process, differential track settlement could be predicted.

5.4 Beam element models

A slab track consists of several layers, see Figs. 2.4 and 2.6. Each of these layers can be seen as a relatively slender structural part. In this thesis, different kinds of models have been developed, wherein the so-called beam element models, the rail, panel and possibly also the roadbed are described using Rayleigh–Timoshenko beam elements. In addition, when transition zones are analysed, also the sleepers are modelled using Rayleigh–Timoshenko beam elements.

In **Paper A**, two types of slab track models are considered, see Figs. 5.1 and 5.2. In Fig. 5.1, the slab is modelled by one continuous layer of beam elements, and in Fig. 5.2 the concrete parts are modelled by two layers of beam elements. In the two-layer slab model, the upper layer containing the discrete slab panels is described by (coupled or decoupled) beams of a given length. The bottom beam layer (panel for the track model shown in Fig. 5.1 and roadbed for the track model shown in Fig. 5.2) is supported by non-interacting springs and dampers (Winkler foundation). The load from the vehicle is assumed to be symmetrically distributed between the two rails and, therefore, only half of the slab and one rail need to be considered.

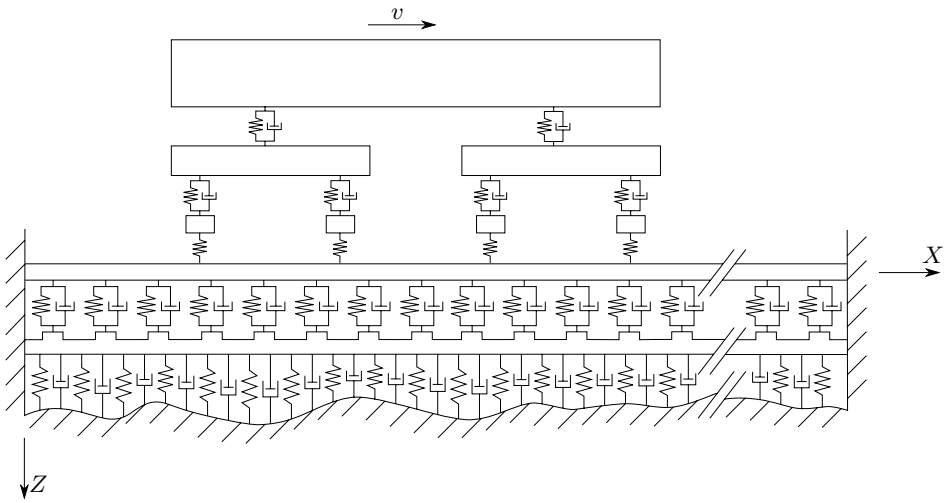

Figure 5.1: Sketch of track and vehicle models where the slab is modelled as one continuous layer of beam elements. The track model contains two layers of beams: rail and concrete panel. The concrete panel is supported by a Winkler foundation, where the prescribed (possibly random) variation in stiffness is indicated by the irregular ground surface.

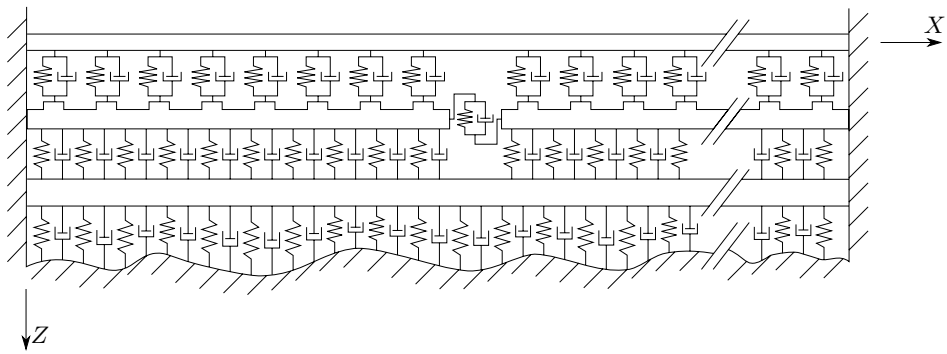

Figure 5.2: Sketch of track model where the slab is modelled as two layers of beam elements. The model contains three layers of beams: rail, discrete panels of concrete slab and continuous concrete roadbed. The concrete base is supported by a Winkler foundation.

In **Paper B**, transition zones are studied, and the slab track model shown in Fig. 5.1 is combined with the ballasted track model developed by Nielsen and Igeland [38], see Fig. 5.3. By solving a multi-objective optimisation problem, the dynamic loads on the track are minimised with respect to selected track design parameters.

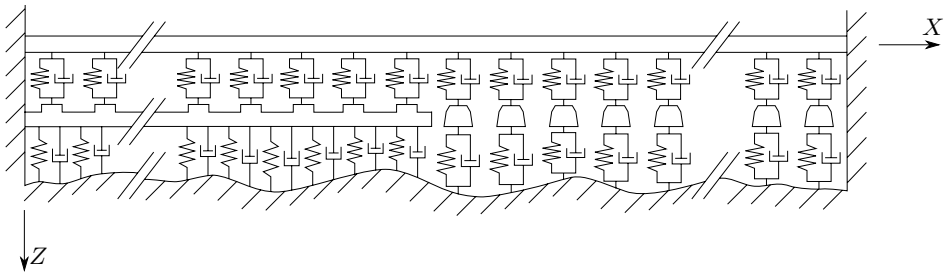

Figure 5.3: Sketch of complete track model with transition zone. The track model contains rail, sleepers and panel that are modelled as Rayleigh–Timoshenko beam elements. The sleepers and panel are supported by a Winkler foundation.

5.5 Shell and solid element models

In this thesis, the three-dimensional (3D) model is developed in Abaqus using Python scripts, see Fig. 5.4. By using a 3D model including both of the rails, the effects of non-symmetric loading and track irregularities can be assessed. In the 3D model, the rails are modelled using Rayleigh–Timoshenko beam elements, while the concrete panel and roadbed are modelled using either shell or solid elements.

The 3D parameterised model is developed using the so-called Application Programming Interface (API) within Abaqus. The API offers direct communication to the kernel meaning that the Abaqus/CAE graphical user interface (GUI) is bypassed [66]. Hence, the system matrices of the track are generated by running the Python script using the API.

Independently if scripts or the GUI is used, the performed actions are recorded in a replay file (consisting of Python code). Hence, if a Python-command is not known, it can be executed in the GUI and the corresponding Python code can then be found in the replay file. By using this approach, it is straightforward to extend the Python script. Furthermore, Python commands can be directly typed into the Abaqus GUI, which can be used to verify that the code works as intended.

Python scripts in Abaqus is a powerful tool to develop detailed track models. One of the most beneficial features is that it is very easy to change a wide range of different settings. Within this thesis, a range of different types of models has been developed with different dimensions, mesh densities, rail pad models, etc. By just changing one option in the code, a completely different track model can be generated.

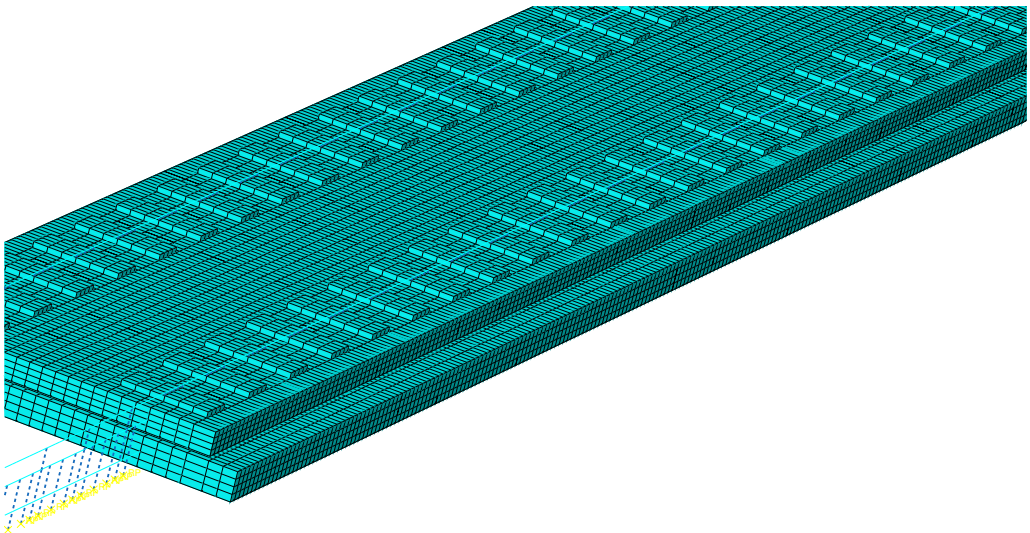

Figure 5.4: Parameterised 3D slab track model developed in Abaqus using Python scripts (from **Paper C**).

When the system matrices have been generated from the Python scripts in Abaqus, they are exported to Matlab where the dynamic vehicle–track interaction simulation is conducted using an in-house software (see Sec. 5.7 for more information). From this simulation, the time history of the vertical wheel–rail contact force at each wheel is obtained. In order to obtain the corresponding time history of the stress distribution in the concrete parts and the pressure on the foundation, the contact forces are used as input to a new dynamic simulation in Abaqus. Due to the moving character of these forces, the time-variant position of where each wheel–rail contact force shall be applied will in most time steps be located in between two rail nodes of the track model. By using the same shape functions as were used in the dynamic simulation in Matlab (see Eq. (5.7)), the force and moment that shall be applied on each of the two adjacent rail nodes can be determined.

When the dynamic simulation is conducted in Abaqus, there are several different solution options available. In this thesis, the so-called implicit dynamic and modal dynamic options have been used. The implicit dynamic approach is valid for both linear and non-linear problems, whereas the modal dynamic approach can be a cost-efficient option for linear problems. In **Paper C** – **Paper E**, a 3D linear track model was used, which makes the modal dynamic approach a valid and applicable option. Note that it has been verified that the two options give similar results for linear track models.

In Fig. 5.5, the different steps of the methodology are shown. In particular, it is highlighted which software is used in each step. The first step in Fig. 5.5(a), in which the 3D model is generated, can be divided into several substeps, see Fig. 5.5(b).

As an example of the results obtained from the dynamic simulation in Abaqus, Fig. 5.6 shows the maximum principal stress due to bending at a specific instant in time. When this stress field was calculated, a non-symmetric measured track irregularity profile was applied. From the figure, stress concentrations can be seen around the current locations of the wheels. In particular, the stress levels are increased below the locations of the rail seats where the load from the vehicle is transferred from the rail to the panel.

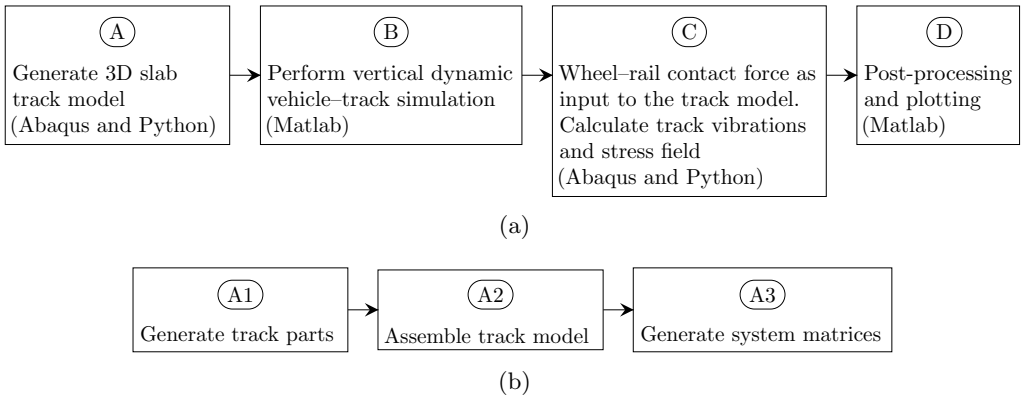

Figure 5.5: Flowchart of (a) the different steps in the simulation methodology and (b) the substeps when the 3D slab track model is generated (from **Paper C**).

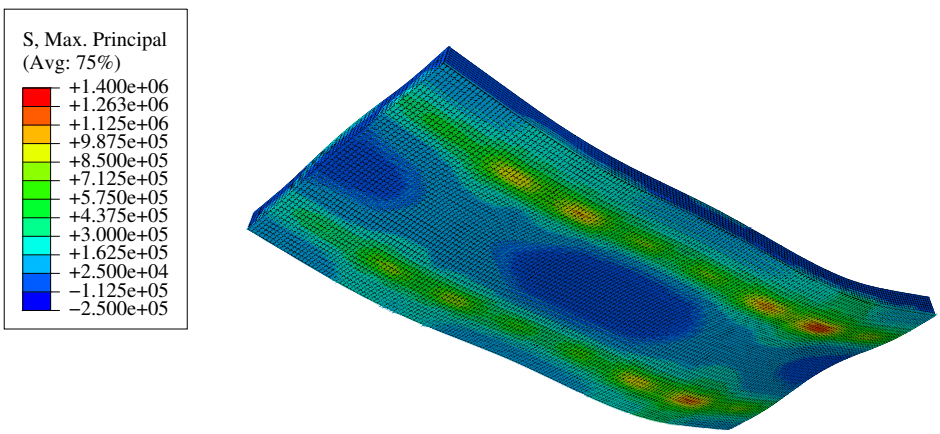

Figure 5.6: Maximum principal stress distribution due to bending on the bottom side of the concrete panel at one time instant. The displacements in the figure are enlarged with a factor of 3000 (from **Paper C**).

5.6 Vehicle models

In this thesis, a range of different vehicle models has been employed spanning from simple wheelset models to advanced 3D models that include bogies and a car body. There are advantages and disadvantages with all models. A disadvantage with a wheelset model (only accounting for the unsprung mass) is that the influence of the suspensions and the inertia of the bogies and car body are neglected. On the other hand, when bogies and a car body are included in the model, the length of the track model has to be increased which increases the computational cost of the model. The benefits of including the car body and secondary suspensions when the focus is on the dynamic response of the track are, generally, small since the secondary suspension acts as a dynamic filter isolating the car body from the bogies in the frequency range where the dynamics of the track is significant ($20 < f < 1500$ Hz) [33].

The fact that a simpler vehicle model can be used in many situations while still obtaining similar results as a more advanced vehicle model is further analysed in **Paper B**. In Fig. 5.7, the wheel–rail contact force and the pressure on the foundation were calculated when the vehicle is passing a transition zone (from slab track to ballasted track). The so-called "Full vehicle model" consists of four wheelsets, two bogies and one car body, see Fig. 5.1. In the bogie model, two wheelsets in one bogie were considered, while the influence of the car body was accounted for by a static point force acting at the centroid of the bogie. From Fig. 5.7, it can be seen that both vehicle models give similar results. In this thesis, the bogie model has been used frequently. The model is a good trade-off between simpler and more advanced models: The computational time for a bogie model is not increased significantly compared to a wheelset model, and the track responses are similar to those obtained with more advanced vehicle models.

In this thesis, the vehicle is always modelled as a multibody system. When the vehicle model is derived, the standard physical degrees-of-freedom (DOFs) are collected in a vector $\boldsymbol{x}_{\mathrm{b}}^{\mathrm{v}}$ (superscript v indicates vehicle). The number of DOFs in $\boldsymbol{x}_{\mathrm{b}}^{\mathrm{v}}$ varies depending on what vehicle model that is applied. In addition to the DOFs included in $\boldsymbol{x}_{\mathrm{b}}^{\mathrm{v}}$, an auxiliary massless DOF, interfacing with the track, is introduced at each wheel. This is used in the constraint equations. By collecting these massless DOFs in a vector $\boldsymbol{x}_{\mathrm{a}}^{\mathrm{v}}$, the equations of motion for the vehicle can be written as

$$\begin{aligned}\begin{bmatrix}\mathbf{0} & \mathbf{0}\\ \mathbf{0} & \boldsymbol{M}_{\mathrm{bb}}^{\mathrm{v}}\end{bmatrix}\begin{Bmatrix}\ddot{\boldsymbol{x}}_{\mathrm{a}}^{\mathrm{v}}(t)\\ \ddot{\boldsymbol{x}}_{\mathrm{b}}^{\mathrm{v}}(t)\end{Bmatrix}+\begin{bmatrix}\mathbf{0} & \mathbf{0}\\ \mathbf{0} & \boldsymbol{C}_{\mathrm{bb}}^{\mathrm{v}}\end{bmatrix}\begin{Bmatrix}\dot{\boldsymbol{x}}_{\mathrm{a}}^{\mathrm{v}}(t)\\ \dot{\boldsymbol{x}}_{\mathrm{b}}^{\mathrm{v}}(t)\end{Bmatrix}\\ +\begin{bmatrix}\boldsymbol{K}_{\mathrm{aa}}^{\mathrm{v}} & \boldsymbol{K}_{\mathrm{ab}}^{\mathrm{v}}\\ \boldsymbol{K}_{\mathrm{ba}}^{\mathrm{v}} & \boldsymbol{K}_{\mathrm{bb}}^{\mathrm{v}}\end{bmatrix}\begin{Bmatrix}\boldsymbol{x}_{\mathrm{a}}^{\mathrm{v}}(t)\\ \boldsymbol{x}_{\mathrm{b}}^{\mathrm{v}}(t)\end{Bmatrix}+\begin{Bmatrix}\boldsymbol{F}_{\mathrm{a}}(t)\\ \mathbf{0}\end{Bmatrix}=\begin{Bmatrix}\mathbf{0}\\ \boldsymbol{F}_{\mathrm{b}}^{\mathrm{ext}}\end{Bmatrix},\end{aligned} \tag{5.1}$$

where $\boldsymbol{K}_{\mathrm{aa}}^{\mathrm{v}}$ contains the stiffness coupling between the massless DOFs interacting with the track and the wheelset DOFs, $\boldsymbol{F}_{\mathrm{a}}(t)$ includes contact forces between the wheel(s) and the rail(s) and $\boldsymbol{F}_{\mathrm{b}}^{\mathrm{ext}}$ contains all external forces (in this thesis only gravity loads). The contact between wheel and rail is modelled as a non-linear Hertzian spring, which allows for momentary loss of contact. The Hertzian contact stiffness is determined by

$$k_{\mathrm{H}i} = C_{\mathrm{H}}\langle x_{\mathrm{b}i} - x_{\mathrm{a}i}\rangle^{1/2}, \quad i = 1, 2, \ldots, N, \tag{5.2}$$

where N is the number of wheels in the vehicle model, C_{H} is the Hertzian constant and the Macaulay brackets are defined as $\langle \bullet \rangle = \frac{1}{2}(\bullet + |\bullet|)$.

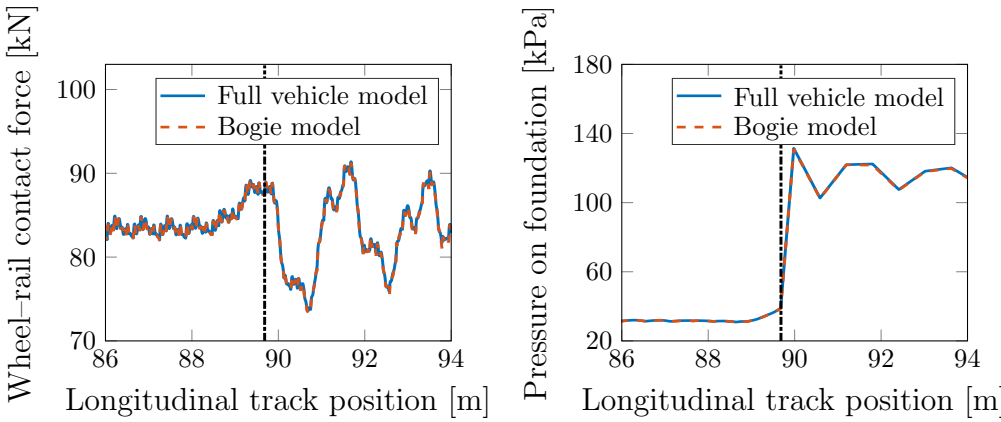

(a) (b)

Figure 5.7: Full vehicle model versus simplified vehicle model considering (a) wheel–rail contact forces for the leading wheelset and (b) pressure between sleeper/panel and foundation. On the ballasted track (right of the vertical line) with sleepers at discrete positions, the pressure varies along the lateral direction. In the presented figure, the maximum value is considered. The vertical lines indicate the position of the transition (from **Paper B**).

5.7 Simulation of vertical dynamic train–track interaction

For both the 2D and 3D track models, the methodology used to simulate the vertical dynamic vehicle–track interaction is similar. Since the vehicle is modelled as a multibody system, while the track is modelled using finite elements, the number of degrees-of-freedom (DOFs) for the vehicle model is negligible compared to the number of DOFs for the track model. Hence, the modal reduction is only applied for the track DOFs.

Let $\boldsymbol{x}^{\mathrm{t}}(t)$ be a vector containing the track DOFs and let $\boldsymbol{F}^{\mathrm{t}}(t)$ contain the external loads (superscript t denotes track). In this thesis, the external loads acting on the track consists of the wheel–rail contact force $\boldsymbol{F}_{\mathrm{a}}(t)$. The equations of motion for the track can be written as

$$\boldsymbol{A}^{\mathrm{t}}\dot{\boldsymbol{y}}^{\mathrm{t}}(t) + \boldsymbol{B}^{\mathrm{t}}\boldsymbol{y}^{\mathrm{t}}(t) = \begin{Bmatrix} \boldsymbol{F}^{\mathrm{t}}(t) \\ \boldsymbol{0} \end{Bmatrix}, \tag{5.3}$$

where

$$\boldsymbol{y}^{\mathrm{t}}(t) = \begin{Bmatrix} \boldsymbol{x}^{\mathrm{t}}(t) \\ \dot{\boldsymbol{x}}^{\mathrm{t}}(t) \end{Bmatrix}, \ \boldsymbol{A}^{\mathrm{t}} = \begin{bmatrix} \boldsymbol{C}^{\mathrm{t}} & \boldsymbol{M}^{\mathrm{t}} \\ \boldsymbol{M}^{\mathrm{t}} & \boldsymbol{0} \end{bmatrix}, \ \boldsymbol{B}^{\mathrm{t}} = \begin{bmatrix} \boldsymbol{K}^{\mathrm{t}} & \boldsymbol{0} \\ \boldsymbol{0} & -\boldsymbol{M}^{\mathrm{t}} \end{bmatrix}. \tag{5.4}$$

Here, $\boldsymbol{K}^{\mathrm{t}}$, $\boldsymbol{C}^{\mathrm{t}}$ and $\boldsymbol{M}^{\mathrm{t}}$ are the stiffness, damping and mass matrices of the track. From the equations of motion, the corresponding eigenvalue problem can be written as

$$\begin{bmatrix} \boldsymbol{K}^{\mathrm{t}^{-1}}\boldsymbol{C}^{\mathrm{t}} & \boldsymbol{K}^{\mathrm{t}^{-1}}\boldsymbol{M}^{\mathrm{t}} \\ -\mathbf{I} & \mathbf{0} \end{bmatrix} \begin{Bmatrix} \underline{\boldsymbol{\rho}}^{(n)} \\ \mathrm{i}\underline{\omega}_n\underline{\boldsymbol{\rho}}^{(n)} \end{Bmatrix} = -\frac{1}{\mathrm{i}\underline{\omega}_n} \begin{Bmatrix} \underline{\boldsymbol{\rho}}^{(n)} \\ \mathrm{i}\underline{\omega}_n\underline{\boldsymbol{\rho}}^{(n)} \end{Bmatrix}, \tag{5.5}$$

where $\underline{\omega}_n$ are angular eigenfrequencies, $\underline{\boldsymbol{\rho}}^{(n)}$ are eigenvectors and $\mathbf{I}$ denotes the unit matrix (underline indicates a complex-valued quantity). From the solution of the eigenvalue problem, the modal matrix, $\boldsymbol{P}$, can be assembled. The modal matrix works as a mapping between the spatial and modal domains as

$$\boldsymbol{y}^{\mathrm{t}}(t) = \underline{\boldsymbol{P}}\underline{\boldsymbol{q}}^{\mathrm{t}}(t), \tag{5.6}$$

where $\underline{\boldsymbol{q}}^{\mathrm{t}}$ are the modal displacements.

In order to couple the track and vehicle models, constraint equations need to be established. In this thesis, third-degree interpolation polynomials derived from Rayleigh–Timoshenko beam theory are employed. By letting $\beta_j = 12EI_{\mathrm{r}}/(kGA_{\mathrm{r}}l_j^2)$ and $\xi_j \in [0\ l_j]$ be the local coordinate of rail element j with length l_j, the interpolation polynomials are given by, [67],

$$\begin{aligned}
N_{1j} &= \frac{1}{1+\beta_j}\Big(1 - \frac{3\xi_j^2}{l_j^2} + \frac{2\xi_j^3}{l_j^3}\Big) + \frac{\beta_j}{1+\beta_j}\Big(1 - \frac{\xi_j}{l_j}\Big), \\
N_{2j} &= \frac{1}{1+\beta_j}\Big(-\frac{\xi_j}{l_j} + \frac{2\xi_j^2}{l_j^2} - \frac{\xi_j^3}{l_j^3}\Big)l_j + \frac{\beta_j}{1+\beta_j}\Big(\Big[-\frac{\xi_j}{l_j} + \frac{\xi^2}{l_j^2}\Big]\frac{l_j}{2}\Big), \\
N_{3j} &= \frac{1}{1+\beta_j}\Big(\frac{3\xi_j^2}{l_j^2} - \frac{2\xi_j^3}{l_j^3}\Big) + \frac{\beta_j}{1+\beta_j}\frac{\xi}{l_j}, \\
N_{4j} &= \frac{1}{1+\beta_j}\Big(\frac{\xi_j^2}{l_j^2} - \frac{\xi_j^3}{l_j^3}\Big)l_j + \frac{\beta_j}{1+\beta_j}\Big(\Big[\frac{\xi}{l_j} - \frac{\xi^2}{l_j^2}\Big]\frac{l_j}{2}\Big).
\end{aligned} \tag{5.7}$$

The track and vehicle models are coupled via the constraint equation, [68],

$$\boldsymbol{x}_{\mathrm{a}}^{\mathrm{v}}(t) = \boldsymbol{N}\underline{\boldsymbol{P}}^{\mathrm{int}}\underline{\boldsymbol{q}}^{\mathrm{t}}(t) + \boldsymbol{x}^{\mathrm{irr}}, \tag{5.8}$$

where $\boldsymbol{x}^{\mathrm{irr}}$ contains the prescribed wheel/rail irregularity, $\underline{\boldsymbol{P}}^{\mathrm{int}}$ is the time-variant partition of the modal matrix corresponding to the rail DOFs that are adjacent to the current position of the vehicle DOFs, and $\boldsymbol{N}$ is a time-variant block matrix containing the interpolation polynomials given in Eq. (5.7).

To solve the vertical dynamic vehicle–track interaction, a mixed extended state-space vector $\underline{\boldsymbol{z}}$ is defined as

$$\underline{\boldsymbol{z}} = \{\underline{\boldsymbol{q}}^{\mathrm{tT}} \quad \boldsymbol{x}_{\mathrm{a}}^{\mathrm{vT}} \quad \boldsymbol{x}_{\mathrm{b}}^{\mathrm{vT}} \quad \dot{\boldsymbol{x}}_{\mathrm{a}}^{\mathrm{vT}} \quad \dot{\boldsymbol{x}}_{\mathrm{b}}^{\mathrm{vT}} \quad \hat{\boldsymbol{F}}_{\mathrm{a}}^{\mathrm{T}}\}^{\mathrm{T}}, \tag{5.9}$$

where $\hat{\boldsymbol{F}}_{\mathrm{a}} = \int \boldsymbol{F}_{\mathrm{a}}(t)\mathrm{d}t$. This state-space vector is used to derive a coupled, time-variant system which is given by

$$\underline{\boldsymbol{A}}(\underline{\boldsymbol{z}}, t)\dot{\underline{\boldsymbol{z}}} + \underline{\boldsymbol{B}}(\underline{\boldsymbol{z}}, t)\underline{\boldsymbol{z}} = \underline{\boldsymbol{F}}(\underline{\boldsymbol{z}}, t), \tag{5.10}$$

where the vector $\underline{\boldsymbol{F}}$ and the matrices $\underline{\boldsymbol{A}}$ and $\underline{\boldsymbol{B}}$ are defined in Eq. (15) in **Paper A**. By rewriting Eq. (5.10) as an initial value problem which can be solved numerically in the time domain, the time-history of the state-space vector is obtained. For more information about the modal description of the track model, and how it is used to calculate the wheel–rail contact forces, see **Paper A** and Ref. [38].

From the solved extended state-space vector, a range of track responses can be determined. In particular, the time-history of the wheel–rail contact force at each wheel can be extracted by differentiation of the state-space vector. In this thesis, if shell or solid elements are used, the calculated time history of the wheel–rail contact force at each wheel is used as input to a post-processing dynamic simulation in Abaqus to for example calculate the stresses in the concrete parts or the pressure on the foundation, see Sec. 5.5. If all finite element parts are instead described using beam elements, cf. **Paper A** and **Paper B**, the track responses are calculated by post-processing operations based on the state-space vector. In particular, the pressure $P(X, Y, t)$ on the foundation is calculated as

$$P(X, Y, t) = k_{\mathrm{f}}(X, Y)\boldsymbol{N}(\xi)\boldsymbol{n}(t) + c_{\mathrm{f}}(X, Y)\boldsymbol{N}(\xi)\dot{\boldsymbol{n}}(t), \tag{5.11}$$

where X and Y denote the longitudinal and lateral directions and k_{f} and c_{f} are the bed modulus and viscous damping of the foundation at the given element. Further, $\boldsymbol{n}$ contains the physical displacements and rotations (including the quasistatic contribution from the truncated modes) at the two beam element nodes adjacent to the coordinate where the pressure is evaluated. As an example, Fig. 5.8 shows the pressure between sleeper/slab and foundation before and after an optimisation of transition zone design to reduce the maximum pressure.

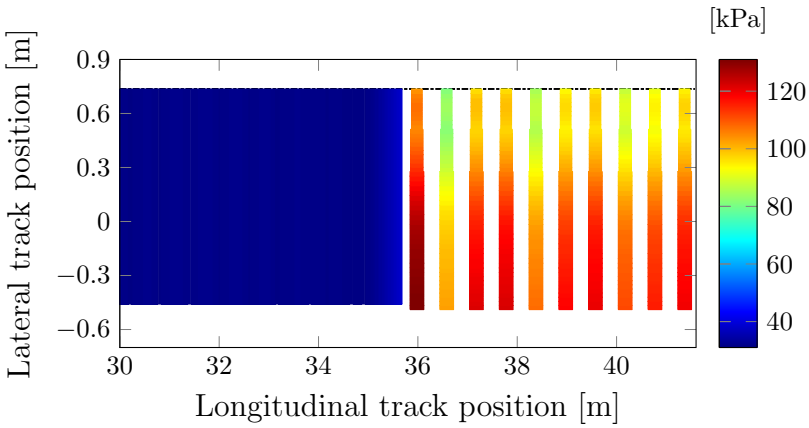

(a)

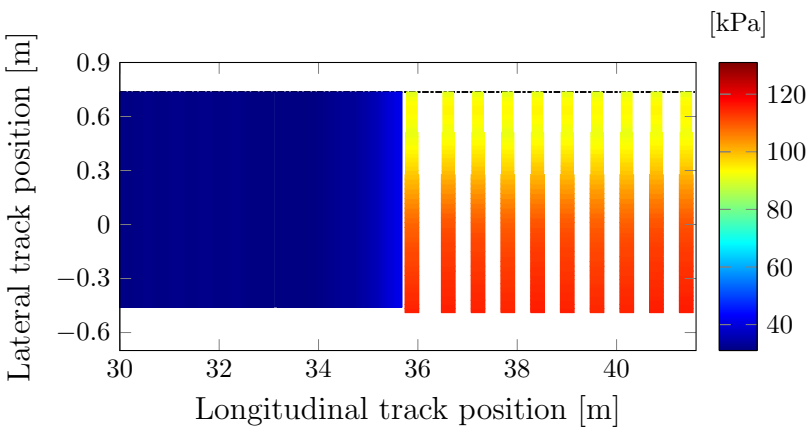

(b)

Figure 5.8: Distribution of maximum pressure between sleeper/panel and foundation for (a) the nominal track and (b) the track that has been optimised to minimise the maximum pressure between sleeper/panel and foundation. The horizontal lines at lateral track position $Y = 0.75$ m indicate the symmetry lines of the track, while the rail is located along $Y = 0$ m (from **Paper B**).

6 Concrete structures

For the analysis of concrete structures, the models adopted in the literature span from analytical calculations to detailed (non-linear) three-dimensional (3D) finite element (FE) models. To determine which modelling technique that shall be used, it is important to consider to which detail the concrete fracture process shall be modelled and how to account for the interaction between reinforcement and concrete. Furthermore, the application and the response that shall be calculated affect how advanced model that is required. As an example, a more advanced model is required if the crack pattern shall be evaluated, as compared to a case when only the overall behaviour of the structure, e.g. maximum load-bearing capacity, is assessed.

For the interaction between reinforcement and concrete, the modelling techniques employed may be divided into three levels of complexity. The simplest one is called embedded reinforcement [69]. Here, full bond between the concrete and reinforcement is assumed. In an FE model, the influence of the reinforcement is then included by simply increasing the density and stiffness of the concrete elements where the reinforcement bars are present. Embedded reinforcement can be used when the overall behaviour of a structure is being analysed. However, if the embedded reinforcement technique is used, the predicted crack pattern will not be realistic. A more comprehensive approach, which accurately determines the crack pattern, is to account for slip between concrete and reinforcement. The reinforcement can then be represented by 1D bars, and reinforcement and concrete are connected through so-called interface elements. When using such a model, a bond-slip relation is used as a constitutive relation of the interface. In the most comprehensive approach, the reinforcement and concrete are described using 3D solid elements, and they are connected using 2D interface elements that incorporate a friction model.

To simulate cracking of concrete, the two most commonly used approaches are (i) the discrete crack approach and (ii) the smeared crack approach [70]. In a discrete crack approach, the crack discontinuity is usually described by special elements in which a constitutive relation between stress and crack opening is used. In a smeared crack approach, continuum elements are typically employed, and it is assumed that the crack discontinuity is smeared out over the elements. The strain that is associated with the cracking will then be localised into continuum elements. With this approach, no individual cracks will be resolved, only cracked regions. Both the discrete crack approach and the smeared crack approach have certain advantages and disadvantages, which are described in detail in Ref. [70].

As described above, there are a lot of modelling choices when considering concrete structures. As a tool to choose a suitable complexity level of the model, Plos et al. [71] described a multi-level structural assessment strategy. The idea of this approach is that if a structure fulfils its requirements when it is analysed with a simplified (conservative) model, there is no need to develop more advanced models due to the additional working hours and computational time required. However, if the simplified model does not show that the structure fulfils its requirements, actions have to be made. One approach is to

enhance the assessment by subsequently applying more advanced models. In their paper, Plos et al. [71] analysed two different structures with five different models including (i) a simplified (strip) model, (ii) linear FE model and (iii–v) non-linear FE models of varying complexity. The most advanced non-linear FE models were described in detail in Ref. [72], in which modelling strategies were obtained from a range of parameter studies.

In this thesis, the influence of cracks in the concrete parts is analysed in **Paper E**. The main focus is to investigate how the dynamic vehicle–track interaction is affected when cracks are present in the concrete parts. The input that is needed from the model of reinforced concrete to the dynamic model is then the bending stiffness of a cracked section. This response can be estimated using an analytical model of reinforced concrete based on beam theory, see Sec. 6.3, and hence there is no need to develop a detailed non-linear 3D FE model for this application. The model of reinforced concrete is partly based on theory presented in Eurocode 2 [73], which is summarised in Sec. 6.1. In addition, the model of reinforced concrete is used to estimate crack widths, which can be compared to limit values presented in Ref. [74]. A review of research related to concrete structures in railways is presented in Sec. 6.2.

6.1 Eurocode 2

To harmonise technical specifications, the Commission of the European Community decided that an action programme should be developed [75]. This resulted in the so-called Structural Eurocode programme, which consists of a range of different standards in the field of construction. In particular, Eurocode 2 covers the design of concrete structures. In the first part of Eurocode 2, general recommendations for concrete design are presented [73]. In this research, these recommendations are used to account for the influence of creep, see Sec. 6.1.1, and for the calculation of crack widths, see Sec. 6.1.2.

6.1.1 Influence of creep

The influence of creep is essential when considering the long-term effects of concrete structures. One of the most important effects that needs to be included is that the elastic modulus of the concrete will be reduced due to creep. The effective elastic modulus of concrete, $E_{\mathrm{c,eff}}$, can be calculated as, [73],

$$E_{\mathrm{c,eff}} = \frac{E_{\mathrm{c}}}{1 + \varphi(\infty, t_0)}, \tag{6.1}$$

where E_{c} is the nominal elastic modulus of the concrete and $\varphi(\infty, t_0)$ is the final creep value. The final creep value is given by

$$\varphi(\infty, t_0) = \varphi_{\mathrm{RH}} \beta(f_{\mathrm{cm}}) \beta(t_0), \tag{6.2}$$

where φ_{RH} is a factor to allow for the influence of relative humidity on the final creep value, $\beta(f_{\mathrm{cm}})$ is a factor which varies with the compressive strength of the concrete, f_{cm},

and $\beta(t_0)$ accounts for the age of the concrete at its first loading cycle.

6.1.2 Crack width

According to Eurocode 2 [73], the crack width can be calculated by multiplying the maximum crack spacing with the difference between the mean strain in the reinforcement and the mean strain of the concrete between the cracks. This strain difference can be estimated as

$$\Delta\epsilon_{\mathrm{m}} = \max\Big(\frac{\sigma_{\mathrm{s}} - k_{\mathrm{t}}\frac{f_{\mathrm{ctm}}}{\rho_{\mathrm{p,eff}}}(1+\alpha\rho_{\mathrm{p,eff}})}{E_{\mathrm{s}}},\ 0.6\frac{\sigma_{\mathrm{s}}}{E_{\mathrm{s}}}\Big), \tag{6.3}$$

where σ_{s} is the steel stress, k_{t} is a factor depending on the duration of loading, f_{ctm} is the mean tensile strength of the concrete, E_{s} is the elastic modulus of the steel and α is the ratio between the elastic modulus of the steel and concrete. The factor $\rho_{\mathrm{p,eff}}$ is the ratio between the area of the steel bars and the effective area of concrete in tension surrounding the reinforcement at depth

$$h_{\mathrm{c,eff}} = \min(2.5(h-d), (h-x)/3, h/2), \tag{6.4}$$

where h is the thickness of the structure, d is the distance from the top of the structure to the centroid of the reinforcement in tension (assuming that the bottom of the structure is in tension) and x is the distance from the top of the structure to the neutral axis.

The maximum crack spacing is calculated as

$$s_{\mathrm{r,max}} = k_3 c + k_1 k_2 k_4 \frac{\phi}{\rho_{\mathrm{p,eff}}}, \tag{6.5}$$

where ϕ is the diameter of the reinforcement bar, c is the thickness of the covering concrete layer and k_1, k_2, k_3 and k_4 are parameter values that vary with the reinforcement surface and type of loading. Finally, the crack width, w_{k}, can be calculated as

$$w_{\mathrm{k}} = s_{\mathrm{r,max}}\Delta\epsilon_{\mathrm{m}}. \tag{6.6}$$

6.2 Review of research on concrete structures in railways

In research on railway tracks, the number of reported strength analyses of concrete parts is relatively limited. Rezaie et al. [76] conducted both numerical and experimental analyses to investigate longitudinal cracks in pre-stressed concrete sleepers. In their model, the concrete was represented by solid elements, while the steel bars were described by truss elements. You et al. [77] presented a review of fatigue life assessment methods for prestressed concrete sleepers. In their paper, it was concluded that the fatigue life of sleepers is typically assessed by estimating the dynamic loads and support conditions for the sleeper and calculating the bending moment at critical sections. These bending

moments are then used in a fatigue life criterion considering the material characteristics. By including stochastic variables in a ballasted track model, Rahrovani [78] studied how statistical methods can be used to calculate the probability of failure (PF) of a concrete monobloc sleeper. By conducting multiple simulations of the vehicle–track dynamics, the PF was determined using either Markov chain or Monte Carlo simulations. By using the Nelder-Mead method, the settings of the stochastic variables that resulted in a predefined PF-value could be determined. Finally, analyses of cracks in concrete sleepers have been analysed in several experimental test campaigns [76, 79, 80].

Poveda et al. [48] analysed fatigue due to compressive loads on the concrete panels in a slab track structure. By using measured loads from high-speed trains as input to a linear FE model, the maximum equivalent stress was calculated. Based on Miner's rule and rain flow counting in a critical stress direction, the damage and fatigue life of the concrete panel were determined. The magnitude of the stress intensity factor when considering a through-transverse crack in the roadbed was studied by Zhu et al. [81]. In this study, a simplified 3D model consisting of beam and plate elements was used to calculate the wheel–rail contact forces. The calculated forces were applied as input to a more detailed FE model of the track, where panel, CA (concrete-asphalt) mortar, roadbed and subgrade were all modelled as solid elements. By using the extended finite element method (XFEM), the stress intensity factors at the crack tip in the concrete roadbed could be determined. Zi et al. [82] developed a non-linear FE model to study conical crack formations in concrete sleepers embedded in a slab track system. In compression, the concrete was modelled as a linear elastic material, while a softening plasticity model including a cohesive crack model was used in tension. Finally, Tarifa et al. [83] conducted three-point bending tests on full-scale concrete slabs and identified failure patterns.

6.3 Model of reinforced concrete

Cracks in the concrete parts of a slab track structure can decrease the structural integrity and introduce a risk for reinforcement corrosion. As described in the initial paragraphs of Sec. 6, different modelling strategies spanning from simple hand calculation models to advanced 3D non-linear FE models are used depending on the application. In this thesis, the purpose of the reinforced concrete model is to calculate the bending stiffness of a cracked panel section and to estimate the crack widths. These responses can be determined from a beam model where a uniaxial stress-state and full interaction between concrete and steel are assumed. In the stress analyses, since full bond is assumed, the reinforcement bars can be modelled as concrete with a transformed cross-section. Linear elastic models are used for the concrete in compression and for the steel in both compression and tension. The description of the reinforced concrete model given below is divided into three parts including (i) calculation of bending stiffness (Sec. 6.3.1), (ii) calculation of crack widths (Sec. 6.3.2), and (iii) influence of restraint forces (Sec. 6.3.3).

6.3.1 Bending stiffness

The first step in the calculation model is to determine the location of the neutral axis. This is done by neglecting the influence of the concrete in tension for the cracked section. The same cross-sectional area, A_s, and distance, s, between the reinforcement bars in the lateral and longitudinal directions of the upper and lower reinforcement bars are presumed. For such a double-reinforced section, the distance, x, from the top of the panel to the neutral axis can be determined from the centre of gravity equation, [84],

$$w\Big[\frac{x^2}{2} + \frac{(\alpha-1)A_\mathrm{s}(x-d_1)}{s} - \frac{\alpha A_\mathrm{s}(d_2-x)}{s}\Big] = 0, \tag{6.7}$$

where α is the ratio between the elastic modulus of the steel and concrete, w is the width of the slab and d_1 and d_2 are the distances from the top of the panel to the upper and lower reinforcements. Note that if long-term effects are taken into account, the effective modulus of elasticity should be used when α is calculated, see Sec. 6.1. When the location of the neutral axis has been determined, it is straightforward to calculate the effective area, A_eff, and moment of inertia, I_eff, as, [84],

$$A_\mathrm{eff} = w[x + (\alpha-1)A_\mathrm{s}/s + \alpha A_\mathrm{s}/s], \tag{6.8a}$$

$$I_\mathrm{eff} = w[x^3/3 + (\alpha-1)A_\mathrm{s}(x-d_1)^2/s + \alpha A_\mathrm{s}(d_2-x)^2/s]. \tag{6.8b}$$

The bending stiffness of the cracked section is calculated as

$$EI_\mathrm{II} = E_\mathrm{c,eff} I_\mathrm{eff}, \tag{6.9}$$

where $E_\mathrm{c,eff}$ is calculated according to Eq. (6.1). Note that if long-term effects are not taken into account, the bending stiffness of a cracked section is calculated similarly, but using the nominal elastic modulus, E_c.

6.3.2 Crack width

In order to estimate crack widths, the steel stresses need to be determined. If shrinkage is taken into account, the shrinkage load, F_cs, is calculated as, [84],

$$F_\mathrm{cs} = E_\mathrm{s}\epsilon_{\mathrm{cs},\infty}A_\mathrm{s}w/s, \tag{6.10}$$

where E_s is the elastic modulus of the steel, while $\epsilon_{\mathrm{cs},\infty}$ is the total final shrinkage strain calculated according to Eurocode 2 [73]. From the shrinkage load, the concrete stress at depth z measured from the neutral axis can be determined by Navier's formula as

$$\sigma_{\mathrm{c},\infty}(z) = \frac{F_\mathrm{cs}}{A_\mathrm{eff}} + \frac{F_\mathrm{cs}e_\mathrm{s,eff} + M}{I_\mathrm{eff}}z, \tag{6.11}$$

where $e_\mathrm{s,eff} = d_2 - x$ and M is the applied moment. When the concrete stress is known, the steel stress is calculated as

$$\sigma_\mathrm{s} = -\frac{F_\mathrm{cs}s}{A_\mathrm{s}w} + \alpha\sigma_{\mathrm{c},\infty}(z_\mathrm{s}), \tag{6.12}$$

where z_s is the distance between the lower reinforcement and the neutral axis. Finally, the crack width, w_k, is calculated based on theory outlined in Eurocode 2 [73], see Sec. 6.1, as

$$w_k = s_{r,max}\Delta\epsilon_m, \tag{6.13}$$

where $s_{r,max}$ is the maximum crack spacing, while $\Delta\epsilon_m$ is the difference between the mean strain in the reinforcement and the mean strain of the concrete between the cracks.

6.3.3 Influence of restraint forces

For a concrete structure that is constrained to move due to interaction with an interfacing structure, restraint forces will occur. In the calculations described above, the influence of such restraint forces is neglected. For the concrete panel in a slab track, it is difficult to determine the restraint degree, which may vary between different designs. Therefore, the approach taken here is to perform the calculations with either no restraint or full restraint to obtain the bounds for each response.

When full restraint is assumed, the steel stress due to the restraint, $\sigma_{s,res}$, can be estimated using the following deformation condition, [85],

$$\frac{\sigma_{s,res}A_s + F_{cs}}{E_{c,eff}A_{I,eff}}l_{res} + n_{cr}w_{m,c}(\sigma_{s,res}) - \epsilon_{cs}l_{res} = 0, \tag{6.14}$$

where l_{res} is the length between the restraints, n_{cr} is the number of cracks between the restraints, while $w_{m,c}$ is the crack width when having cyclic or sustained loading and taking long-term effects into account. Based on a stress-slip relation for long-term response, cf. [86], a conservative estimation of $w_{m,c}$ is given by, [85],

$$w_{m,c} = 0.52\Big(\frac{\phi\sigma_{s,res}^2}{0.22f_{cm}E_s}\Big) + \frac{4\sigma_{s,res}\phi}{E_s}. \tag{6.15}$$

The steel stress contribution due to the restraint is calculated using an iterative approach. By setting $n_{cr} = 1$, $\sigma_{s,res}$ is evaluated using Eqs. (6.14)–(6.15). The total steel stress when assuming full restraint, $\sigma_{s,tot}$, can then be calculated as

$$\sigma_{s,tot} = \sigma_s + \sigma_{s,res}. \tag{6.16}$$

From the total steel stress, the restraint force, F_{res}, is calculated as

$$F_{res} = \frac{\sigma_{s,tot}A_s w}{s}. \tag{6.17}$$

If the restraint force is larger than the cracking load, $N_{cr} = f_{ctm}A_{I,eff}$, a new crack will form and the calculation is repeated with $n_{cr} = 2$. This iterative process of successively increasing the number of cracks is continued until the restraint force is lower than the cracking load, which implies that no new cracks will form. For more information about the restraint force model, see Refs. [85, 86].

7 Model validation

The calibration and validation of simulation models against measurements are essential. Depending on what parts of the slab track that are calibrated and/or validated, the measurement strategy varies. To analyse the dynamics of a structure, it is common to use an impact hammer (including an integrated force transducer) to excite the structure in a Single-Input Multiple-Output (SIMO) test. The response is typically measured using piezoelectric accelerometers [20, 87].

A range of different slab track models has been calibrated using measurements. In a study by Cox et al. [88], a dynamic characterisation of different floating slab track systems and direct fixation fastening systems was performed by measuring receptances (displacement over force) in a full-scale test rig. In the test, 12 m long rails were used and boxes of sand were placed at the ends to reduce boundary effects. Another full-scale test rig was presented by Wang et al. [12]. In their study, the dynamic performance of the China Railway Track System (CRTS) series was analysed by conducting so-called wheel-drop tests. Zangeneh et al. [89] analysed the dynamic response of portal frame railway bridges and used a model updating approach to calibrate their FE model. Sainz-Aja et al. [90] calibrated a slab track model based on finite elements by using measured data from a full-scale test rig. The measurements included variations of load amplitude and frequency, with a focus on low frequencies up to 5.6 Hz. Although there are several benefits of conducting measurements in a lab, e.g. easier to control track properties and better track availability, dynamic track models have also been calibrated based on field measurements [91–93].

The presented three-dimensional (3D) slab track model has been calibrated and validated using hammer impact measurements in a full-scale test rig. The measurements were performed in the State Key Laboratory of Traction Power at the Southwest Jiaotong University in Chengdu, P.R. China. For more information about the test rig, see **Paper D** and Refs. [12, 94]. In **Paper D**, measured frequency response functions (FRFs) were compared with the corresponding simulated FRFs. In the model calibration, the stiffness of the rail pad was calibrated using a parameter study. The remaining unknown parameters, i.e. the damping of the rail pad and stiffness and damping of the soil, were calibrated using a Genetic Algorithm (GA). In Fig. 7.1, the different steps in the GA are shown. For more information about the GA, see Sec. 8.1.

For multiple other excitation positions, which were not included in the calibration, it was found that the model captures the trend of the SIMO measurements with rather small deviations compared to the overall dynamic range. This implies that the 3D model can successfully represent the dynamics of the test rig and can be considered as validated. In Fig. 7.2, a typical example of measurement versus simulation from the validation is shown.

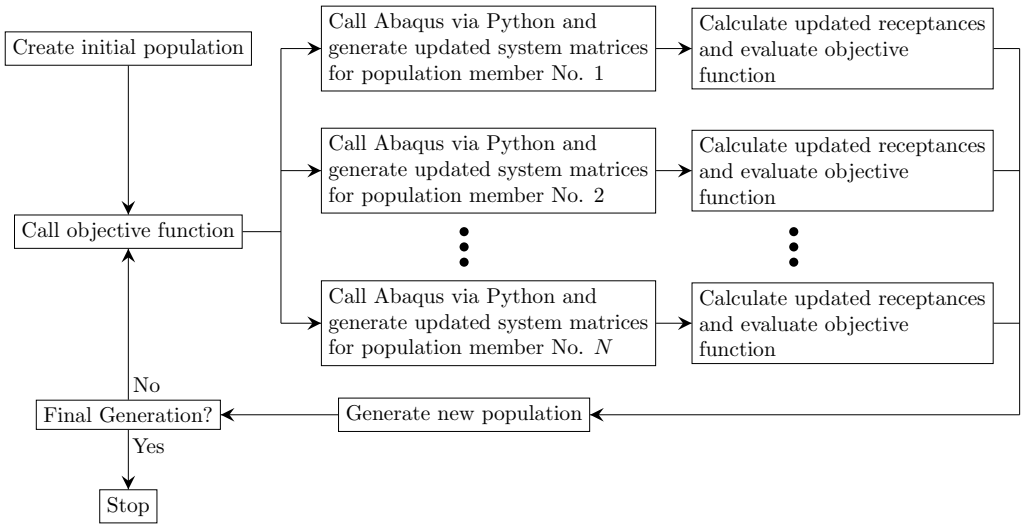

Figure 7.1: Flowchart of the GA that is applied to calibrate the 3D model (from **Paper D**).

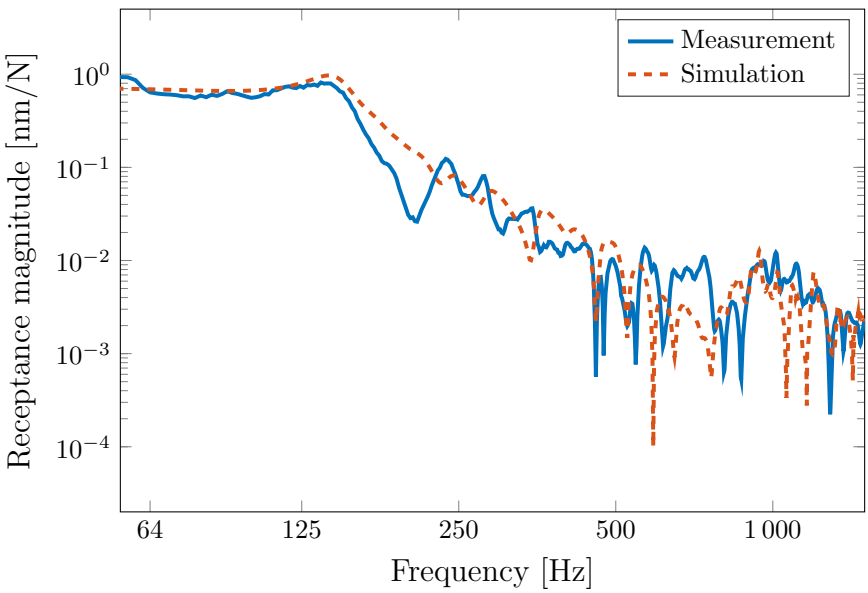

Figure 7.2: Validation results comparing the receptances from measurement and simulation for excitation on the rail between two rail seats and measuring/calculating the response on the panel (from **Paper D**).

8 Optimisation

In this thesis, different kinds of optimisation procedures have been employed. In **Paper B**, a multi-objective optimisation problem is solved using a Genetic Algorithm (GA) called the Non-dominated Sorting Genetic Algorithm II (NSGA-II). The strengths of GAs are also utilised in **Paper D**, where a single-objective optimisation problem is solved in the calibration process for the 3D model. In addition, a gradient-based optimisation procedure is used in **Paper E** for the optimisation of slab track design. In this chapter, GAs are briefly discussed in Sec. 8.1, while the NSGA-II is described in Sec. 8.2. Finally, some alternatives to GAs are covered in Sec. 8.3.

8.1 Genetic algorithms

For the optimisation of several engineering problems, continuous methods and Response Surface Methodology (see Sec. 8.3) may fail [95]. Typical reasons are several objective functions, high computational cost and complexity of the objective function(s). A typical remedy is to implement a heuristic method, where the use of Genetic Algorithms (GAs) is one of the most applied methodologies. In GAs, the optimisation problem is solved by mimicking evolutionary phenomena in nature. All GAs have (similar to Darwinian natural selection) some kind of heredity, variation and selection.

When a GA is applied, the members (also called chromosomes) in the first generation are usually selected randomly [95]. Each member is then assigned a fitness value(s) based on the evaluation of the objective function(s). The general idea is that a member with a higher fitness value has a higher probability of being part of the next generation. Producing the next generation is typically made by crossover (mixing two members from the previous generation) and mutation (adding more variation to the next generation). In **Paper D**, the standard GA implemented in Matlab is used in the calibration process for the 3D model. In Fig. 7.1, the different steps in the GA are highlighted.

8.2 Non-dominated Sorting Genetic Algorithm II

In **Paper B**, the Non-dominated Sorting Genetic Algorithm II (NSGA-II) developed by Deb et al. [96] is employed. The algorithm can be described as follows: Initially, a parent population is generated randomly, and an offspring population is created based on binary tournament selection, recombination and mutation operators. Each member is assigned a fitness value corresponding to its non-domination rank. The non-domination rank is determined by a non-dominated sorting approach that calculates non-dominated fronts. The best fronts are used to build up the next generation until all seats in the generation are occupied, which implies that elitism is ensured. Regarding the final front that is used to fill the last seats in the next generation, all members in the front will not

fit, and a crowding distance control function is used to determine which members shall be used. The crowding distance control function is defined to preserve diversity among the solutions. The generation of a new generation is shown schematically in Fig. 8.1.

One iteration in NSGA-II has computational complexity $\mathcal{O}(MN^2)$, where M is the number of objective functions and N is the population size. This is significantly faster than its precursor NSGA, cf. [97]. In **Paper B**, the evaluation of the objective functions is the most computationally demanding step, and it has to be performed for each member in each generation. The computational cost is, however, reduced by using parallel computations for each generation.

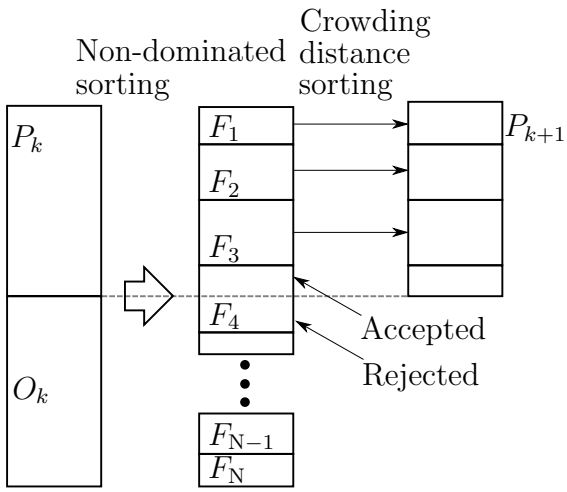

Figure 8.1: Scheme of how NSGA-II works. P_k and O_k denote the k^{th} parent and offspring generations, while $F_1, F_2, \ldots, F_N$ denote the non-dominated fronts. Based on Fig. 2 in Ref. [96] (from **Paper B**).

8.3 Alternatives to genetic algorithms

Classical continuous optimisation problems are typically solved with gradient-based algorithms, e.g. Newton's method (and modifications of it) or the steepest descent method [98]. The solution strategy for all gradient-based algorithms can be divided into several steps: initialisation, find descent direction, perform line search, update, and termination check. Typically, the challenges with these types of algorithms are to determine the descent direction and step length. Depending on the used algorithm, the objective function is often required to be in $\mathcal{C}^1$ (or even $\mathcal{C}^2$). Other drawbacks with gradient-based algorithms are that only one objective function can be used per simulation and that a calculated minimum is not necessarily a global minimum if convexity of the objective function is not

ensured [98].

In optimisation problems, where the gradient cannot be calculated and expressed in closed form, the gradient can be calculated approximately using finite difference methods, e.g. forwards, backwards or central difference methods. In **Paper E**, the gradient-based non-linear programming solver *fmincon* in Matlab is used. It utilises an interior point algorithm and a forward difference method, and the Hessian is estimated using the Broyden–Fletcher–Goldfarb–Shanno (BFGS) algorithm [99].

An alternative approach when the gradient cannot be calculated is to use a so-called Response Surface Methodology (RSM). In this method, the objective function is approximated with a meta-model, typically consisting of polynomials or splines (piecewise polynomial functions), and a regression model is used to fit the meta-model to the objective function. As soon as the coefficients of the meta-model have been determined, the objective function can be expressed approximately by the meta-model, and continuous optimisation techniques can be used. Since the objective function based on the meta-model is smooth, the optimal solution can be calculated. Furthermore, an approximate solution to the original problem is obtained. In a post-processing stage, statistical methods can be used to estimate how good the fit of the meta-model is compared to the original objective function. As examples, Shevtsov et al. [100] and Nielsen and Fredö [101] used methodologies that are based on RSM in order to optimise railway wheels, while Lundqvist and Dahlberg [102] used RSM to optimise the dynamic component of the wheel–rail contact forces with respect to the foundation bed modulus.

9 Summary of appended papers

Paper A: Simulation of vertical dynamic vehicle–track interaction using a two-dimensional slab track model

The vertical dynamic interaction between a railway vehicle and a slab track is simulated in the time domain using an extended state-space vector approach in combination with a complex-valued modal superposition technique for the linear, time-invariant and two-dimensional track model. Wheel–rail contact forces, bending moments in the concrete panel, and load distributions on the supporting foundation are evaluated. Two generic slab track models including one or two layers of concrete slabs are presented. Rail receptances for the two slab track models are compared with the receptance of a conventional ballasted track. The described procedure is demonstrated by two application examples involving: (i) the periodic response due to the rail seat passing frequency as influenced by the vehicle speed and a foundation stiffness gradient, and (ii) the transient response due to a discrete rail irregularity.

Paper B: Multi-objective optimisation of transition zones between slab track and ballasted track using a genetic algorithm

For a transition zone between ballasted track and slab track, the vertical dynamic vehicle–track interaction due to the track stiffness gradient is simulated in the time domain using the extended state-space vector approach described in **Paper A**. By considering a multi-objective optimisation problem solved by a genetic algorithm, the maximum dynamic loads on the track structure are minimised with respect to the selected design variables. From the solution of the optimisation problem, non-dominated fronts of the objective functions are obtained illustrating potential for a significant reduction of the dynamic loads. The influence of the length of the transition zone on the maximum dynamic loads is discussed. Since the transition zones are optimised neglecting the influence of wheel and rail irregularities, a methodology is proposed to evaluate the robustness of the optimal design by evaluating its performance when periodic rail irregularities with different combinations of wavelength and phase, relative to the position of the transition, are applied in the model.

Paper C: Simulation of vertical dynamic vehicle–track interaction using a three-dimensional slab track model

The simulation methodology presented in **Paper A** is extended to a three-dimensional (3D) model. The track model is generated in Abaqus using Python scripts, from which the system matrices are exported to Matlab where the simulation of dynamic vehicle–track interaction is conducted. The wheel–rail contact forces obtained from this simulation are used as input to a post-processing simulation in Abaqus to determine the time-varying stress field of the concrete parts and the pressure on the foundation. From an extensive convergence study, recommendations for element type and mesh discretisation are given for a range of track responses. The 3D model is compared to the 2D model presented in **Paper A**, and it is concluded in which situations the 2D model is sufficient and in which scenarios the 3D model is required. The influence of vehicle speed on the wheel–rail

contact forces, and the influence of support stiffness irregularities on the overall track stiffness, are investigated.

Paper D: Calibration and validation of the dynamic response of two slab track models using data from a full-scale test rig

The three-dimensional model presented in **Paper C** is calibrated and validated against impact hammer measurements. Single-Input-Multiple-Output (SIMO) measurements were conducted by exciting the rail and measuring the response of the concrete panel and roadbed. The measured frequency responses functions (FRFs) are compared with the corresponding calculated FRFs from the 3D model. The calibration consists of two steps including (i) a parameter study and (ii) a genetic algorithm. The calibrated model captures the trend of the measurements with rather small deviations compared to the overall dynamic range. This implies that the model can successfully represent the dynamic response of the test rig and can be considered as validated.

Paper E: Optimisation of slab track design considering dynamic train–track interaction and environmental impact

In the design of a slab track, there is a delicate balance between having a robust, high-quality track and the environmental and economic costs of having an overdesigned solution. In this paper, the calculation method presented in the European standard 16432-2 is used to optimise slab track design with the objective to minimise the environmental footprint. Design parameters included in the optimisation consist of different types of concrete in the panel, and the height and width of the panel and roadbed. Based on the optimised design, simulations of dynamic vehicle–track interaction are conducted (using the 3D slab track model presented in **Paper C**) to investigate if the design can be trimmed even further. In parallel, a model of reinforced concrete has been developed to predict crack widths and the bending stiffness of a cracked panel section. The reduced bending stiffness is used as input to the dynamic model to investigate the influence of cracks in the concrete panel on significant track responses. The model of reinforced concrete is also used to assess whether the amount of steel reinforcement in the slab track design can be reduced, which will reduce the environmental footprint from slab track even further.

10 Contributions of the thesis

The current thesis contributes to the development of a methodology for the simulation and optimisation of vertical dynamic vehicle–slab track interaction. The contributions include:

- Development of (i) a two-dimensional (2D) slab track model (**Paper A**) (ii) a transition zone model between slab track and ballasted track (**Paper B**) and a three-dimensional (3D) slab track model (**Paper C**).
- Development of an optimisation methodology that can be used for the design of transition zones (**Paper B**).
- Investigation of the influence of the selection of vehicle model on significant track responses such as the wheel–rail contact force and the pressure on the foundation (**Paper B**).
- Investigation of the influences of a range of parameters, such as rail pad stiffness, geometric dimensions of the concrete parts, vehicle speed, soil stiffness and irregularities in the longitudinal level, on significant track responses (**Paper A** – **Paper C**).
- Assessment of the influence of mesh discretisation and selection of element type in the finite element model of the track on computational accuracy (**Paper C**).
- Execution of hammer impact measurements on a full-scale slab track test rig with subsequent calibration and validation of a 3D slab track model (**Paper D**).
- Implementation of a model of reinforced concrete and the static calculation analysis presented in the European standard 16432-2 (**Paper E**).
- Development of an optimised slab track design with the objective to minimise the environmental footprint from the concrete parts (**Paper E**).

11 Future work

As to future work, the presented models, and in particular the calibrated and validated three-dimensional (3D) slab track model, can be used in a range of investigations. Since this track model is parameterised using Python, it is straightforward to extend it and investigate the dynamic performance of other types of slab track designs. In particular, the influence of applying more non-conventional slab track designs, e.g. using a so-called ladder structure, can be studied. This type of track modelling opens up for future optimisation, where the design can be optimised such that concrete and reinforcement are only used in areas where really needed.

The transition zone model can be used to analyse differential settlement. Today, the development of differential settlement is typically simulated by combining a short-term dynamic model with a long-term empirical settlement model [65, 103]. By using the presented transition zone model to calculate the short-term response, differential settlement of transition zones can be simulated. Furthermore, the parameterised 3D slab track model can be extended to a 3D transition zone model including two rails and concrete parts described using beam, shell or solid elements. With such a detailed 3D transition zone model, the impact of having e.g. auxiliary rails, longer sleepers, an approaching slab and/or variations in soil conditions on vehicle and track dynamics can be assessed. The detailed transition zone model can also be used for calibration/validation of the transition zone model presented in **Paper B**.

In the 3D slab track model developed in this thesis, the concrete parts are described using a linear elastic material model. By extending the model with a non-linear material model, crack patterns can be studied. If this should be simulated, the full bond assumption between concrete and steel cannot be used any longer. Hence, the reinforcements need to be explicitly modelled using finite elements and a bond-slip relation between concrete and steel needs to be adopted, see Sec. 6. In addition, the impact of having prestressed panels and including alternative concrete types, e.g. steel-fibre reinforced concrete, can be assessed.

Finally, only vertical dynamics has been studied in this thesis. The dynamic vehicle–track interaction model can be extended to include also lateral and longitudinal dynamics. For a ballasted track, some initial work has been conducted [104, 105]. With such an extension of the 3D slab track model, the performance of slab tracks in curves and the effect of lateral track misalignment on significant track responses can be analysed.

References

[1] UIC (International Union of Railways). High speed rail brochure – 2018. (2018).

[2] In2Rail. Deliverable D3.3, Evaluation of optimised track systems. (2017).

[3] C. Esveld. Modern railway track. MRT-productions, Zaltbommel. (2001).

[4] P.-E. Gautier. Slab track: Review of existing systems and optimization potentials including very high speed. *Construction and Building Materials*. **92** (2015), 9–15.

[5] I Avramovic, ÖBB-Porr. (Private communication). April (2018).

[6] EN 16432-2:2017 CEN Standard. Railway applications – Ballastless track systems – Part 2: System design, subsystems and components. (2017).

[7] UIC (International Union of Railways). High speed rail brochure. (2015).

[8] C. Esveld. Recent developments in slab track. *European Railway Review*. **9**(2) (2003), 81–85.

[9] Capacity4Rail. Public deliverable D 1.1.1, Design requirements and improved guidelines for design (track loading resilience & RAMS). (2014).

[10] S. R. Matias and P. A. Ferreira. Railway slab track systems: Review and research potentials. *Structure and Infrastructure Engineering*. **16**(12) (2020), 1635–1653.

[11] In2Track. Deliverable D3.2, Enhanced track design solutions through predictive analyses. (2019).

[12] M. Wang, C. Cai, S. Zhu and W. Zhai. Experimental study on dynamic performance of typical nonballasted track systems using a full-scale test rig. *Proceedings of the Institution of Mechanical Engineers, Part F: Journal of Rail and Rapid Transit*. **231**(4) (2017), 470–481.

[13] UIC International Railway Solution (IRS). IRS 70727 Railway Application – Track superstructure decision making. Draft 2.0. (2020).

[14] Y. Bezin, D. Farrington, C. Penny, B. Temple and S. Iwnicki. The dynamic response of slab track constructions and their benefit with respect to conventional ballasted track. *Vehicle System Dynamics*. **48**(S1) (2010), 175–193.

[15] Y.-C. Shiau, M.-T. Wang, C.-M. Huang and L.-T. Lu. New model of cement product – Precast slab track for THSR (Taiwan High Speed Rail). *The 25th International Symposium on Automation and Robotics in Construction*, Vilnius, Lithuania. (2008), 129–140.

[16] K. Ando, M. Sunaga, H. Aoki and O. Haga. Development of slab tracks for Hokuriku Shinkansen line. *Quarterly Report of RTRI*. **42**(1) (2001), 35–41.

[17] A. Ekberg and B. Paulsson. INNOTRACK: Concluding Technical Report. International Union of Railways (UIC). (2010).

[18] R. L. Milford and J. M. Allwood. Assessing the CO2 impact of current and future rail track in the UK. *Transportation Research Part D: Transport and Environment.* **15**(2) (2010), 61–72.

[19] K. Zandi, K. Lundgren and I. Lövgren. Ballastless track – Minimizing the climate impact, Tech. rep., Department of Architecture and Civil Engineering, Chalmers University of Technology, Gothenburg, Sweden (2021), 1–50.

[20] D. Thompson. Railway noise and vibration: Mechanisms, modelling and means of control. Elsevier, Oxford. (2008).

[21] J. Theyssen. Modelling the acoustic performance of slab tracks. Licentiate thesis. Department of Architecture and Civil Engineering. Chalmers University of Technology, Gothenburg, Sweden. (2020).

[22] The United Nations. Transforming our world: The 2030 agenda for sustainable development. (2015).

[23] A. Paixão, E. Fortunato and R. Calçada. Design and construction of backfills for railway track transition zones. *Proceedings of the Institution of Mechanical Engineers, Part F: Journal of Rail and Rapid Transit.* **229**(1) (2015), 58–70.

[24] R. Sañudo, L. Dell'Olio, J. Casado, I. Carrascal and S. Diego. Track transitions in railways: A review. *Construction and Building Materials.* **112** (2016), 140–157.

[25] M. Shahraki, C. Warnakulasooriya and K. J. Witt. Numerical study of transition zone between ballasted and ballastless railway track. *Transportation Geotechnics.* **3** (2015), 58–67.

[26] D. Connolly, G. Kouroussis, O. Laghrouche, C. Ho and M. Forde. Benchmarking railway vibrations – Track, vehicle, ground and building effects. *Construction and Building Materials.* **92** (2015), 64–81.

[27] M. Li, E. Berggren, M. Berg and I. Persson. Assessing track geometry quality based on wavelength spectra and track–vehicle dynamic interaction. *Vehicle System Dynamics.* **46**(S1) (2008), 261–276.

[28] N. Correa, O. Oyarzabal, E. G. Vadillo, J. Santamaria and J. Gomez. Rail corrugation development in high speed lines. *Wear.* **271**(9–10) (2011), 2438–2447.

[29] EN 13848-6 CEN Standard. Railway applications – Track – Track geometry quality – Part 6: Characterisation of track geometry quality. (2014).

[30] W. Zhai and S. Zhu. Track design, dynamics and modelling. *Handbook of Railway Vehicle Dynamics (2nd Edition).* Ed. by S. Iwnicki, M. Spiryagin, C. Cole and T. McSweeney. (2020), 307–344.

[31] G. Kouroussis, D. P. Connolly and O. Verlinden. Railway-induced ground vibrations – A review of vehicle effects. *International Journal of Rail Transportation.* **2**(2) (2014), 69–110.

[32] J. Malmborg, P. Persson and K. Persson. Effects of modeling strategies for a slab track on predicted ground vibrations. *Soil Dynamics and Earthquake Engineering.* **136** (2020), 106254.

[33] K. Knothe and S. Grassie. Modelling of railway track and vehicle/track interaction at high frequencies. *Vehicle System Dynamics.* **22**(3–4) (1993), 209–262.

[34] S. Timoshenko. Method of analysis of statical and dynamical stresses in rail. *Proceedings of the Second International Congress of Applied Mechanics*, Zurich, Switzerland. (1926), 12–17.

[35] S. Grassie and S. Cox. The dynamic response of railway track with flexible sleepers to high frequency vertical excitation. *Proceedings of the Institution of Mechanical Engineers, Part D: Transport Engineering.* **198**(2) (1984), 117–124.

[36] S. Grassie, R. Gregory, D. Harrison and K. Johnson. The dynamic response of railway track to high frequency vertical excitation. *Journal of Mechanical Engineering Science.* **24**(2) (1982), 77–90.

[37] Y.-H. Lin and M. Trethewey. Finite element analysis of elastic beams subjected to moving dynamic loads. *Journal of Sound and Vibration.* **136**(2) (1990), 323–342.

[38] J. C. O. Nielsen and A. Igeland. Vertical dynamic interaction between train and track – Influence of wheel and track imperfections. *Journal of Sound and Vibration.* **187**(5) (1995), 825–839.

[39] W. Zhai and X. Sun. A detailed model for investigating vertical interaction between railway vehicle and track. *Vehicle System Dynamics.* **23**(S1) (1994), 603–615.

[40] B. Ripke and K. Knothe. Simulation of high frequency vehicle-track interactions. *Vehicle System Dynamics.* **24** (1995), 72–85.

[41] W. Zhai, K. Wang and C. Cai. Fundamentals of vehicle–track coupled dynamics. *Vehicle System Dynamics.* **47**(11) (2009), 1349–1376.

[42] P. Galvín, A. Romero and J. Domínguez. Fully three-dimensional analysis of high-speed train–track–soil-structure dynamic interaction. *Journal of Sound and Vibration.* **329**(24) (2010), 5147–5163.

[43] W. Zhai, S. Wang, N. Zhang, M. Gao, H. Xia, C. Cai and C. Zhao. High-speed train–track–bridge dynamic interactions – Part II: Experimental validation and engineering application. *International Journal of Rail Transportation.* **1**(1-2) (2013), 25–41.

[44] J. Sadeghi, A. Khajehdezfuly, M. Esmaeili and D. Poorveis. Investigation of rail irregularity effects on wheel/rail dynamic force in slab track: Comparison of two and three dimensional models. *Journal of Sound and Vibration.* **374** (2016), 228–244.

[45] J. Yang, S. Zhu and W. Zhai. A novel dynamics model for railway ballastless track with medium-thick slabs. *Applied Mathematical Modelling.* **78** (2020), 907–931.

[46] J. Luo, S. Zhu and W. Zhai. Development of a track dynamics model using Mindlin plate theory and its application to coupled vehicle-floating slab track systems. *Mechanical Systems and Signal Processing*. **140** (2020), 106641.

[47] Z. Li and T. Wu. Modelling and analysis of force transmission in floating-slab track for railways. *Proceedings of the Institution of Mechanical Engineers, Part F: Journal of Rail and Rapid Transit*. **222**(1) (2008), 45–57.

[48] E. Poveda, C. Y. Rena, J. C. Lancha and G. Ruiz. A numerical study on the fatigue life design of concrete slabs for railway tracks. *Engineering Structures*. **100** (2015), 455–467.

[49] X. Lei and J. Wang. Dynamic analysis of the train and slab track coupling system with finite elements in a moving frame of reference. *Journal of Vibration and Control*. **20**(9) (2014), 1301–1317.

[50] S. Zhu, C. Cai and P. D. Spanos. A nonlinear and fractional derivative viscoelastic model for rail pads in the dynamic analysis of coupled vehicle–slab track systems. *Journal of Sound and Vibration*. **335** (2015), 304–320.

[51] J. Zhang, Y. Zhao, Y. Zhang, X. Jin, W. Zhong, F. W. Williams and D. Kennedy. Non-stationary random vibration of a coupled vehicle–slab track system using a parallel algorithm based on the pseudo excitation method. *Proceedings of the Institution of Mechanical Engineers, Part F: Journal of Rail and Rapid Transit*. **227**(3) (2013), 203–216.

[52] J. Sadeghi, A. Khajehdezfuly, M. Esmaeili and D. Poorveis. Dynamic interaction of vehicle and discontinuous slab track considering nonlinear Hertz contact model. *Journal of Transportation Engineering*. **142**(4) (2016), 04016011.

[53] X. Yang, S. Gu, S. Zhou, J. Yang, Y. Zhou and S. Lian. Effect of track irregularity on the dynamic response of a slab track under a high-speed train based on the composite track element method. *Applied Acoustics*. **99** (2015), 72–84.

[54] S. Zhu, J. Yang, C. Cai, Z. Pan and W. Zhai. Application of dynamic vibration absorbers in designing a vibration isolation track at low-frequency domain. *Proceedings of the Institution of Mechanical Engineers, Part F: Journal of Rail and Rapid Transit*. **231**(5) (2017), 546–557.

[55] J. Blanco-Lorenzo, J. Santamaria, E. Vadillo and O. Oyarzabal. Dynamic comparison of different types of slab track and ballasted track using a flexible track model. *Proceedings of the Institution of Mechanical Engineers, Part F: Journal of Rail and Rapid Transit*. **225**(6) (2011), 574–592.

[56] Y. Çati, S. Gökçeli, Ö. Anil and C. S. Korkmaz. Experimental and numerical investigation of USP for optimization of transition zone of railway. *Engineering Structures*. **209** (2020), 109971.

[57] B. Zuada Coelho, P. Hölscher, J. Priest, W. Powrie and F. Barends. An assessment of transition zone performance. *Proceedings of the Institution of Mechanical Engineers, Part F: Journal of Rail and Rapid Transit*. **225**(2) (2011), 129–139.

[58] B. Zuada Coelho, J. Priest and P. Hölscher. Dynamic behaviour of transition zones in soft soils during regular train traffic. *Proceedings of the Institution of Mechanical Engineers, Part F: Journal of Rail and Rapid Transit.* **232**(3) (2018), 645–662.

[59] H. Heydari-Noghabi, J. Zakeri, M. Esmaeili and J. Varandas. Field study using additional rails and an approach slab as a transition zone from slab track to the ballasted track. *Proceedings of the Institution of Mechanical Engineers, Part F: Journal of Rail and Rapid Transit.* **232**(4) (2018), 970–978.

[60] X. Lei and L. Mao. Dynamic response analyses of vehicle and track coupled system on track transition of conventional high speed railway. *Journal of Sound and Vibration.* **271**(3) (2004), 1133–1146.

[61] Z. Li and T. Wu. On vehicle/track impact at connection between a floating slab and ballasted track and floating slab track's effectiveness of force isolation. *Vehicle System Dynamics.* **47**(5) (2009), 513–531.

[62] W. Zhai, H. Xia, C. Cai, M. Gao, X. Li, X. Guo, N. Zhang and K. Wang. High-speed train–track–bridge dynamic interactions – Part I: Theoretical model and numerical simulation. *International Journal of Rail Transportation.* **1**(1-2) (2013), 3–24.

[63] T. Xin, Y. Ding, P. Wang and L. Gao. Application of rubber mats in transition zone between two different slab tracks in high-speed railway. *Construction and Building Materials.* **243** (2020), 118219.

[64] J.-A. Zakeri and V. Ghorbani. Investigation on dynamic behavior of railway track in transition zone. *Journal of Mechanical Science and Technology.* **25**(2) (2011), 287–292.

[65] H. Wang and V. Markine. Modelling of the long-term behaviour of transition zones: Prediction of track settlement. *Engineering Structures.* **156** (2018), 294–304.

[66] Abaqus. Abaqus Documentation. Providence, RI, USA: Dassault Systèmes. (2018).

[67] J. H. Sällström. Fluid-conveying damped Rayleigh-Timoshenko beams in transverse vibration analyzed by use of an exact finite element Part II: Applications. *Journal of Fluids and Structures.* **4**(6) (1990), 573–582.

[68] J. C. O. Nielsen and T. J. S. Abrahamsson. Coupling of physical and modal components for analysis of moving non-linear dynamic systems on general beam structures. *International Journal for Numerical Methods in Engineering.* **33**(9) (1992), 1843–1859.

[69] H. Broo, K. Lundgren and M. Plos. A guide to non-linear finite element modelling of shear and torsion in concrete bridges, Tech. rep. Department of Civil and Environmental Engineering. Chalmers University of Technology, Gothenburg, Sweden. (2008), 1–27.

[70] G. Hofstetter and G. Meschke. Numerical modeling of concrete cracking. Springer Science & Business Media. (2011).

[71] M. Plos, J. Shu, K. Zandi and K. Lundgren. A multi-level structural assessment strategy for reinforced concrete bridge deck slabs. *Structure and Infrastructure Engineering*. **13**(2) (2017), 223–241.

[72] J. Shu, D. Fall, M. Plos, K. Zandi and K. Lundgren. Development of modelling strategies for two-way RC slabs. *Engineering Structures*. **101** (2015), 439–449.

[73] EN 1992-1-1 CEN Standard. Eurocode 2: Design of concrete structures – Part 1-1: General rules and rules for building. (2004).

[74] EN 1992-1-1 CEN Standard. Eurocode 2: Design of concrete structures – Concrete bridges – Design and detailing rules. (2005).

[75] EN 1990:2002+A1 CEN Standard. Eurocode: Basis of structural design. (2001).

[76] F. Rezaie, M. Shiri and S. Farnam. Experimental and numerical studies of longitudinal crack control for pre-stressed concrete sleepers. *Engineering Failure Analysis*. **26** (2012), 21–30.

[77] R. You, D. Li, C. Ngamkhanong, R. Janeliukstis and S. Kaewunruen. Fatigue life assessment method for prestressed concrete sleepers. *Frontiers in Built Environment*. **3** (2017), 1–13.

[78] S. Rahrovani. Structural reliability and identification with stochastic simulation. PhD thesis. Department of Applied Mechanics, Chalmers University of Technology, Gothenburg, Sweden, 2016.

[79] S. Kaewunruen and A. M. Remennikov. Progressive failure of prestressed concrete sleepers under multiple high-intensity impact loads. *Engineering Structures*. **31**(10) (2009), 2460–2473.

[80] A. Parvez and S. J. Foster. Fatigue of steel-fibre-reinforced concrete prestressed railway sleepers. *Engineering Structures*. **141** (2017), 241–250.

[81] S. Zhu and C. Cai. Stress intensity factors evaluation for through-transverse crack in slab track system under vehicle dynamic load. *Engineering Failure Analysis*. **46** (2014), 219–237.

[82] G. Zi, S.-J. Lee, S. Y. Jang, S. C. Yang, S.-S. Kim, et al. Investigation of a concrete railway sleeper failed by ice expansion. *Engineering Failure Analysis*. **26** (2012), 151–163.

[83] M. Tarifa, X. Zhang, G. Ruiz and E. Poveda. Full-scale fatigue tests of precast reinforced concrete slabs for railway tracks. *Engineering Structures*. **100** (2015), 610–621.

[84] M. Al-Emrani, B. Engström, M. Johansson and P. Johansson. Bärande konstruktioner – Del 2 [Supporting structures – Part 2, in Swedish], Tech. rep. Department of Civil Engineering and Environmental Engineering, Chalmers University of Technology, Gothenburg, Sweden. (2011), 1–320.

[85] B. Engström. Restraint cracking of reinforced concrete structures, Tech. rep. Department of Civil and Environmental Engineering. Chalmers University of Technology, Gothenburg, Sweden. (2014), 1–165.

[86] J.-P. Jaccoud. Cracking under long term loads or imposed deformations. *CEB Comité Euro International du Béton, Bulletin.* (1997), 143–155.

[87] EN 15461:2008+A1 CEN Standard. Railway applications – Noise emissions – Characterisation of the dynamic properties of track sections for pass by noise measurements. (2010).

[88] S. Cox, A. Wang, C. Morison, P. Carels, R. Kelly and O. Bewes. A test rig to investigate slab track structures for controlling ground vibration. *Journal of Sound and Vibration.* **293**(3–5) (2006), 901–909.

[89] A. Zangeneh, C. Svedholm, A. Andersson, C. Pacoste and R. Karoumi. Dynamic stiffness identification of portal frame bridge–soil system using controlled dynamic testing. *Procedia Engineering.* **199** (2017), 1062–1067.

[90] J. Sainz-Aja, J. Pombo, D. Tholken, I. Carrascal, J. Polanco, D. Ferreño, J. Casado, S. Diego, A. Perez, J. E. A. Filho, A. Esen, T. M. Cebasek, O. Laghrouche and P. Woodward. Dynamic calibration of slab track models for railway applications using full-scale testing. *Computers and Structures.* **228** (2020), 106180.

[91] E. Arlaud, S. Costa D'Aguiar and E. Balmes. Receptance of railway tracks at low frequency: Numerical and experimental approaches. *Transportation Geotechnics.* **9** (2016), 1–16.

[92] C. Alves Ribeiro, R. Calçada and R. Delgado. Calibration and experimental validation of a dynamic model of the train-track system at a culvert transition zone. *Structure and Infrastructure Engineering.* **14**(5) (2018), 604–618.

[93] L. R. Ticona Melo, D. Ribeiro, R. Calçada and T. N. Bittencourt. Validation of a vertical train–track–bridge dynamic interaction model based on limited experimental data. *Structure and Infrastructure Engineering.* **16**(1) (2020), 181–201.

[94] W. Zhai, K. Wang, Z. Chen, S. Zhu, C. Cai and G. Liu. Full-scale multi-functional test platform for investigating mechanical performance of track–subgrade systems of high-speed railways. *Railway Engineering Science.* **28**(3) (2020), 213–231.

[95] M. Wahde. Biologically inspired optimization methods: An introduction. WIT press, Milton Keynes. (2008).

[96] K. Deb, A. Pratap, S. Agarwal and T. Meyarivan. A fast and elitist multiobjective genetic algorithm: NSGA-II. *IEEE Transactions on Evolutionary Computation.* **6**(2) (2002), 182–197.

[97] N. Srinivas and K. Deb. Muiltiobjective optimization using nondominated sorting in genetic algorithms. *Evolutionary Computation.* **2**(3) (1994), 221–248.

[98] M. Patriksson, N. Andréasson, A. Evgrafov, E. Gustavsson and M. Önnheim. Introduction to continuous optimization. Studentlitteratur, Lund. (2013).

[99] R. H. Byrd, J. C. Gilbert and J. Nocedal. A trust region method based on interior point techniques for nonlinear programming. *Mathematical Programming.* **89**(1) (2000), 149–185.

[100] I. Shevtsov, V. Markine and C. Esveld. Optimal design of wheel profile for railway vehicles. *Wear.* **258**(7) (2005), 1022–1030.

[101] J. C. O. Nielsen and C. Fredö. Multi-disciplinary optimization of railway wheels. *Journal of Sound and Vibration.* **293**(3) (2006), 510–521.

[102] A. Lundqvist and T. Dahlberg. Railway track stiffness variation – Consequences and countermeasures. *Proceedings of the 19th IAVSD Symposium of Dynamics of Vehicles on Roads and Tracks (IAVSD2005)*, Milano, Italy. (2005), 1–18.

[103] J. C. O. Nielsen and X. Li. Railway track geometry degradation due to differential settlement of ballast/subgrade – Numerical prediction by an iterative procedure. *Journal of Sound and Vibration.* **412** (2018), 441–456.

[104] C. Andersson and T. Abrahamsson. Simulation of interaction between a train in general motion and a track. *Vehicle System Dynamics.* **38**(6) (2002), 433–455.

[105] P. T. Torstensson and J. C. O. Nielsen. Simulation of dynamic vehicle–track interaction on small radius curves. *Vehicle System Dynamics.* **49**(11) (2011), 1711–1732.